NASA Technical Memorandum 4782

F-15B/Flight Test Fixture II: A Test Bed for Flight Research

David M. Richwine
Dryden Flight Research Center
Edwards, California

National Aeronautics and
Space Administration

Office of Management

Scientific and Technical
Information Program

1996

CONTENTS

TABLES

FIGURES

ABSTRACT

NASA Dryden Flight Research Center has developed a second-generation flight test fixture for use as a generic test bed for aerodynamic and fluid mechanics research. The Flight Test Fixture II (FTF–II) is a low-aspect-ratio vertical fin-like shape that is mounted on the centerline of the F-15B lower fuselage. The fixture is designed for flight research at Mach numbers to a maximum of 2.0. The FTF–II is a composite structure with a modular configuration and removable components for functional flexibility. This report documents the flow environment of the fixture, such as surface pressure distributions and boundary-layer profiles, throughout a matrix of conditions within the F-15B/FTF–II flight envelope. Environmental conditions within the fixture are presented to assist in the design and testing of future avionics and instrumentation. The intent of this document is to serve as a user's guide and assist in the development of future flight experiments that use the FTF–II as a test bed. Additional information enclosed in the appendices has been included to assist with more detailed analyses, if required.

NOMENCLATURE

A_s	FTF–II side area, 3424 in^2
b'	span height from the top of the FTF–II, 32.0 in.
c	chord length from the leading edge of the FTF–II, 107.0 in.
$C_{n\beta}$	static directional stability, deg^{-1}
C_p	pressure coefficient, $(p - p_\infty)/q_\infty$
$C_{p_{max}}$	maximum pressure coefficient
C_p^*	critical pressure coefficient
CAS	control augmentation system
F_{sw}	sway pad reaction load, lbf
F_y	side force, lbf
FTF	Flight Test Fixture (F-104)
FTF–II	Flight Test Fixture II (F-15B)
g	acceleration of gravity
Hp	aircraft indicated altitude, ft
$KCAS$	knots calibrated airspeed
l	reference length with turbulent boundary layer, $x - \Delta x$, in.
M	aircraft indicated Mach number
M_r	maximum local Mach number at rake, $x/c = 0.90$
M_x	moment on FTF–II caused by side loads, in-lbf
M_∞	FTF–II noseboom free-stream Mach number
ORD	Objectives and Research Document
p_w	reference static pressure for rake, lbf/ft^2
p_∞	FTF–II noseboom free-stream static pressure, lbf/ft^2

PCM	pulse code modulation
PSD	power spectral density
q_∞	FTF–II noseboom free-stream dynamic pressure, lbf/ft^2
Re	Reynolds number
rms	root mean square
T	absolute temperature, R
T_f	FTF–II total airstream temperature, x/c = 0.96, R
T_w	local wall temperature for rake, x/c = 0.90, R
u	axial velocity component within the boundary layer, ft/sec
U_r	maximum local velocity for rake, ft/sec
w	width, FTF–II, 8.0 in.
x	distance from leading edge, in.
x/c	percent chord, FTF–II
y	distance from wall, in.
z	distance from leading edge, in.
z/b'	percent span, FTF–II
α	FTF–II noseboom local angle of attack, deg
α_A	aircraft indicated angle of attack, deg
β	FTF–II noseboom local angle of sideslip, deg
δ	boundary-layer thickness, in.
Δx	approximate distance from origin of turbulent flow to nose, 12.84 in. (x/c = 0.12)
ζ	damping ratio
ω_n	undamped natural frequency, rad/sec

INTRODUCTION

In 1963, NASA Dryden Flight Research Center (NASA Dryden) constructed a low-aspect ratio fin-like shape called the Flight Test Fixture (FTF) for installation on the lower fuselage of an F-104 aircraft (fig. 1). Since that time, the FTF has been used as a generic test bed for more than 20 aerodynamic and fluid mechanics research experiments. The capabilities and utility of the FTF have been documented frequently.[1–8] In recent years, NASA Dryden has phased out the aging F-104 aircraft. An effort has subsequently been made to develop a larger and more versatile flight test fixture and identify a new test bed aircraft with expanded capabilities relative to the F-104 FTF. An F-15B airplane was chosen as the test bed aircraft for the new flight test fixture because of its availability at NASA Dryden and potential for good flow quality because of the relatively smooth lower fuselage surface. In addition, the ability of the F-15B airplane to reach Mach 2.0 and its in-flight refueling capability were considered to be very desirable features.

The new flight test fixture was installed on the lower fuselage centerline pylon location of an F-15B aircraft and is called the Flight Test Fixture II (FTF–II) (fig. 2). Envelope expansion of the F-15B/FTF–II configuration was

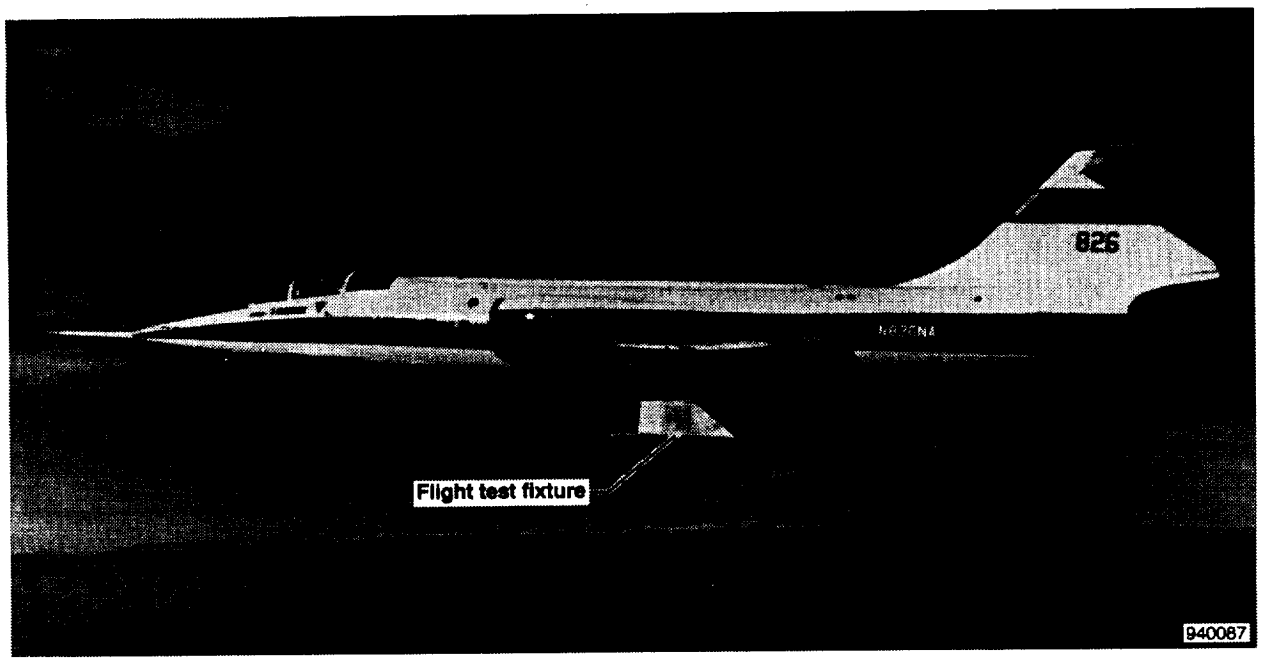

Figure 1. Original FTF installed on the lower fuselage of the F-104 aircraft.

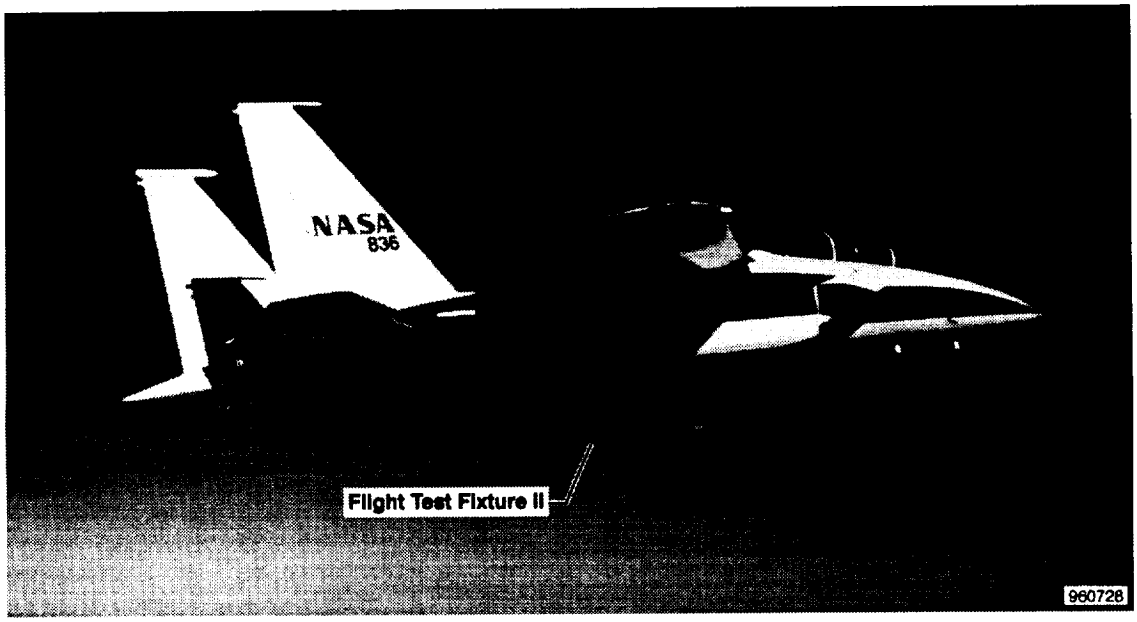

Figure 2. The FTF–II installed on the lower fuselage centerline pylon location of the F-15B aircraft.

completed in a three-phase effort. Phase one consisted of flying the FTF–II uninstrumented on the F-15B airplane to perform envelope-expansion and qualitative flow-quality studies[9] to a maximum of Mach 1.3. Directional stability was evaluated by performing rudder doublets. Flow quality was documented using tufts to define surface flow streamlines.

Phases two (Mach $\leq$ 1.8) and three (Mach > 1.8) were performed with an instrumented FTF–II that included airdata and total temperature probes. The airspeed envelope was expanded to the current aircraft performance and FTF–II design limits of 600 knots calibrated airspeed (*KCAS*) and Mach 2.0. Envelope expansion continued,

including investigations related to directional stability,[10] structures, and aerodynamics. Calibrated load cells were located at the sway brace pads, and preliminary surface pressures were used to monitor in-flight lateral loads and the distribution of these loads. Final envelope expansion of the F-15B/FTF–II configuration was completed in December 1994.

Aerodynamic and environmental characterization of the F-15B/FTF–II began in April 1995. The primary purpose of this report is to document the flow environment of the fixture, such as surface pressure distributions and boundary-layer measurements, throughout a matrix of conditions within the F-15B/FTF–II flight envelope. Environmental conditions within the fixture are presented to assist in the design and testing of future avionics and instrumentation within the fixture. Several guidelines and recommendations are presented to assist in the development of future experiments that may utilize the FTF–II as a test bed.

F-15B AERODYNAMIC TEST BED DESCRIPTION

The NASA F-15B aerodynamic test bed is the combination of the F-15B with the FTF–II installed and is referred to as the F-15B/FTF–II. The following section provides a detailed description of the F-15B/FTF–II configuration, including a description of the F-15B aircraft and capabilities and the FTF–II hardware and instrumentation, and an overview of the flight experiment.

Vehicle Description and Flight Envelope

The NASA F-15B airplane is a two-seat version of the F-15 aircraft, which is a high-performance, supersonic, all-weather, air-superiority fighter built by McDonnell Douglas Aerospace (St. Louis, Missouri).[11] The aircraft is powered by two Pratt & Whitney (West Palm Beach, Florida) F100-PW-100 turbofan engines with afterburners. The F-15B airplane is 63.7 ft long with a 42.8-ft wingspan and a basic operating weight of 27,500 lbm. The aircraft appearance is characterized by a high-mounted swept-back wing, twin vertical stabilizers, and an elevated cockpit to enhance visibility. Primary flight control surfaces consist of conventional ailerons, twin rudders, and stabilators. These surfaces are controlled by a hydromechanical system and an electrical control system called the control augmentation system (CAS).

The F-15B/FTF–II loading is similar to the F-15 Air Superiority "A" loading,[11] with the FTF–II at the centerline tank location. The FTF–II is installed on the F-15B centerline pylon in a manner similar to operational centerline tanks. The maximum projected weight of the FTF–II, including all research systems, is 500 lbm. The FTF–II is smaller, weighs less, and has a lower aerodynamic drag than an empty 610-gal centerline tank that is routinely carried by the F-15 aircraft. As a result, issues such as aircraft stability, performance, and loads were addressed by comparison to the Air Superiority "A" loading for the F-15 aircraft. The FTF–II was designed for flight testing within the operational F-15 airspeed envelope (fig. 3) with an additional limit of Mach 2.0 because of aerodynamic heating considerations on the FTF–II composite structure. Flight testing of the F-15B/FTF–II configuration with the current F100-PW-100 engines shows that steady-state conditions can be achieved at altitudes to a maximum 60,000 ft and airspeeds to a maximum 600 *KCAS* and Mach 2.0.

If airspeeds to the maximum aircraft limits of 800 *KCAS* or Mach 2.3 are desired, further evaluation of several issues would be required. Overall performance of the F-15B airplane would need to be improved with a minimum upgrade to the Pratt & Whitney F100-PW-220 engines. Increased Mach numbers would require the installation of a FTF–II nose section designed for higher levels of aerodynamic heating with an aerodynamic shape more appropriate for improved flow quality at high speeds. Some additional analysis and verification of FTF–II loads and aircraft stability would also be required.

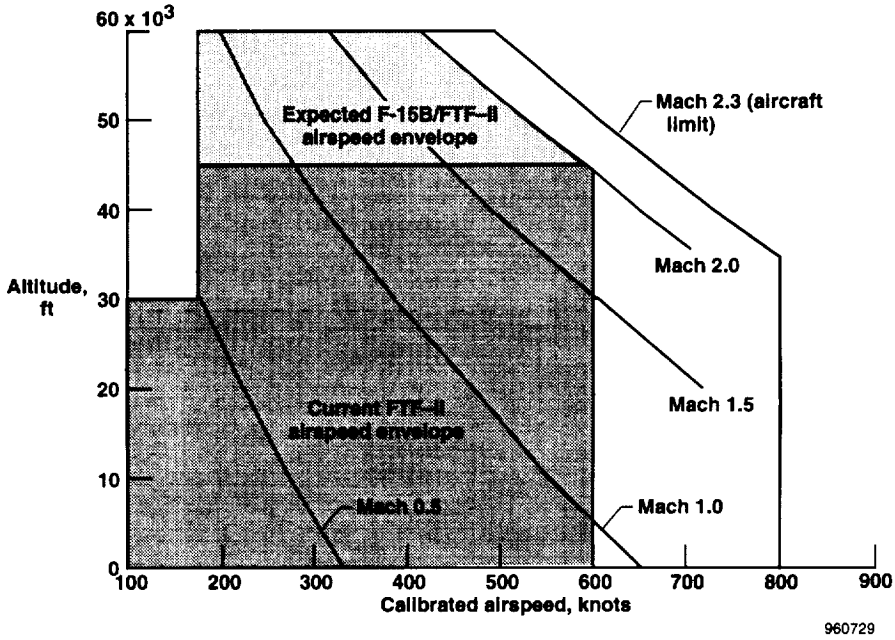

Figure 3. F-15B/FTF–II airspeed limitations.

Flight Test Fixture II Description

The FTF–II is a low-aspect-ratio fin-like shape (fig. 4) 107.0 in. long, 32.0 in. high, and 8.0 in. wide that has an elliptical nose section and blunt trailing base. The FTF–II is a composite modular structure and consists of the basic avionics pylon with a replaceable nose section, side panels, and vertical test article that allow the configuration of the FTF–II to be modified to satisfy a variety of flight test requirements. The upper 19 in. of the FTF–II, the avionics pylon, is a permanent structure that houses avionics, research instrumentation systems, and other support equipment common to most flight experiments. The lower 13 in. of the FTF–II is the vertical test article that, in the current configuration, matches the contour of the upper avionics pylon. The vertical test article is removable and may be replaced by other aerodynamic shapes. Normally, only instrumentation specific to individual research experiments is installed in the lower vertical test article.

All FTF–II side panels are removable with quick internal access through the four left side panels that use external fasteners flush to the surface. The two right side panels extend the length of the fixture and are attached using internal fasteners to minimize discontinuities for aerodynamic experiments such as boundary-layer experiments or surface-flow visualization studies. The elliptical nose section is located in the forward 18.8 in. (one-half major axis) and can be removed independently from either the avionics pylon or the vertical test article. A removable pylon interface fairing and a splitter plate have been installed onto the upper portion of the fixture for improved flow quality. Provisions were also made for a removable 7-in. by 10-in. test panel on the right side of the vertical test article nose section. This test panel has already been used for instrumentation studies that require laminar flow or aerodynamic heating. A removable airdata probe is located at the bottom of the vertical test article nose section.

Instrumentation

The FTF–II data acquisition capability is primarily located in the fixture avionics pylon and uses a 12-bit pulse code modulation system capable of multiplexing data at sample rates as many as 200 samples/sec, depending on the number of data channels. Flight data are transmitted to the ground for storage and postprocessing. A tape recorder

located in the F-15B airplane is used as a backup capability or to record high frequency data if required for a specific flight experiment.

Four load cells (fig. 4(b)) were located at the sway braces to help monitor FTF–II installation preloads and in-flight side loads. Each of the load cells was rated at a maximum of 10,000 lbf compression and oriented to isolate lateral reaction loads as much as possible. Ground calibration load tests were conducted on the F-15B pylon/

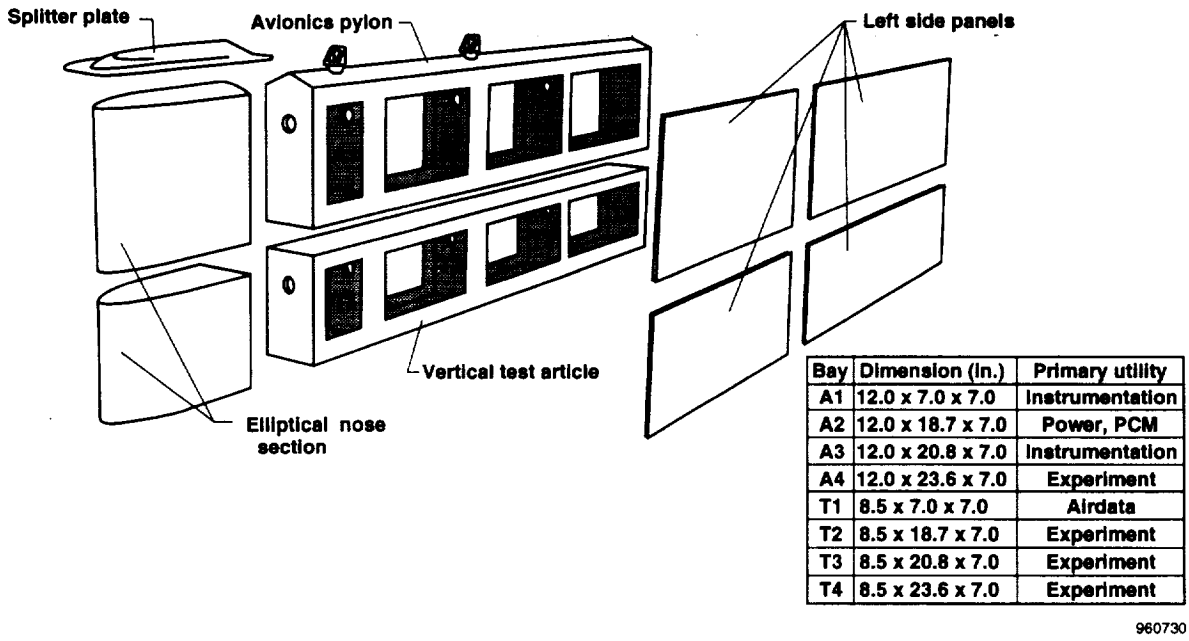

Bay	Dimension (in.)	Primary utility
A1	12.0 x 7.0 x 7.0	Instrumentation
A2	12.0 x 18.7 x 7.0	Power, PCM
A3	12.0 x 20.8 x 7.0	Instrumentation
A4	12.0 x 23.6 x 7.0	Experiment
T1	8.5 x 7.0 x 7.0	Airdata
T2	8.5 x 18.7 x 7.0	Experiment
T3	8.5 x 20.8 x 7.0	Experiment
T4	8.5 x 23.6 x 7.0	Experiment

(a) Exploded isometric view.

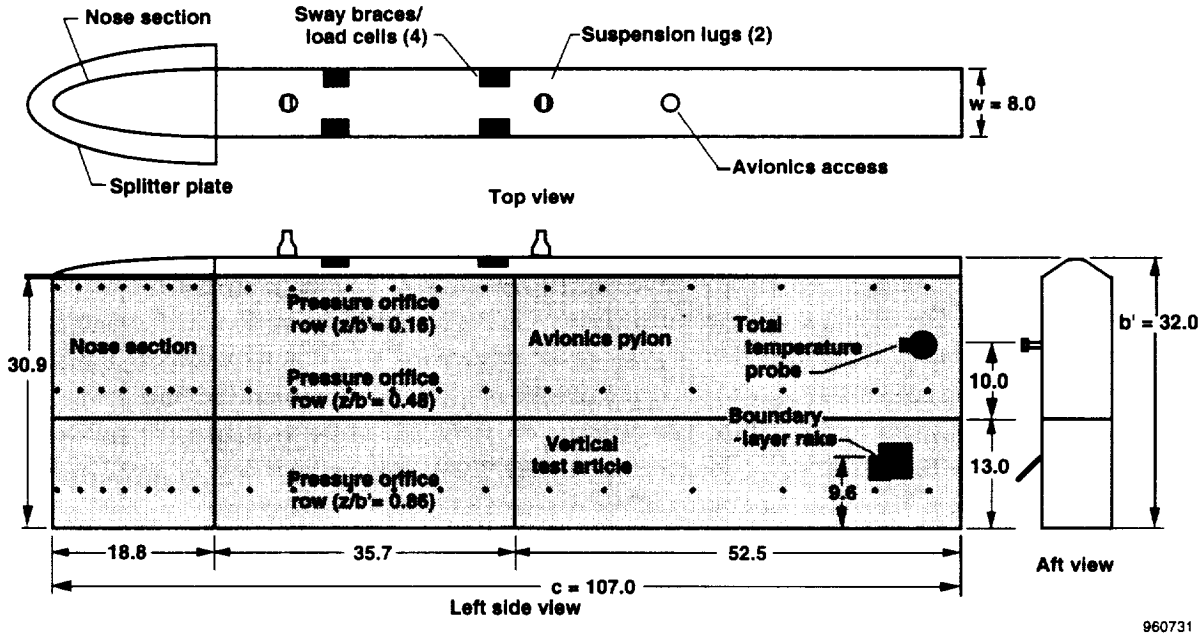

(b) Three view.

Figure 4. FTF–II schematic diagrams.

FTF–II installation to correlate known side loads on the fixture to in-flight loads at the load cells. Appendix A provides details of this ground calibration.

Flush static-pressure orifices (0.030 in. diameter) are located at three spanwise (z/b') locations and distributed chordwise (x/c) (fig. 4(b)). The upper leading edge of the FTF–II was used as the reference $z = 0$ (+ down) and $x = 0$ (+ aft) locations, respectively. The static-pressure orifices are located on both sides of the nose section forward of $x/c = 0.15$ and on only the left side aft of this chord location. A boundary-layer rake located on the left side of the FTF–II (figs. 4(b) and 4(c)) was used to measure boundary-layer profiles at $z/b' = 0.70$ (probe near wall) and $x/c = 0.90$. This rake was canted to accommodate a fine probe resolution near the wall surface (fig. 4(c)) with the

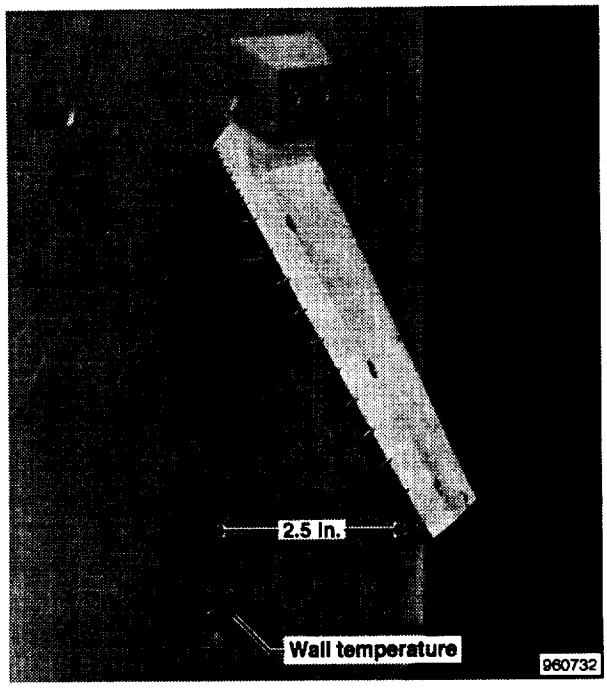

(c) Detail of boundary-layer rake.

Figure 4. Concluded.

outermost probe located 2.5 in. from the surface. Appendix D includes specific probe locations with the tabulated rake data. Pressure measurements were obtained using four temperature-controlled electronic scanning pressure transducers at a sample rate of 6 samples/sec. Surface and rake pressures were measured with ±720 lbf/ft^2 and ±2160 lbf/ft^2 differential transducers, respectively, referenced to the noseboom static pressure with estimated precision within ±3 lbf/ft^2.

Figure 5 shows a removable airdata probe that provides static and total pressure to measure local flow conditions just forward of the fixture. The airdata probe also measures FTF–II noseboom local angle of attack, α, and local angle of sideslip, β. Total temperature is obtained from a probe located on the aft left side of the fixture (fig. 4(b)).

Documentation of acceleration data and internal bay temperatures was conducted to assist with environmental design guidelines for future flight experiments. Accelerometers were located in the bottom of the FTF–II vertical test article midchord to document local three-axis accelerations during various flight conditions. Internal bay temperatures were also obtained to document typical bay temperatures over a variety of ground and flight conditions.

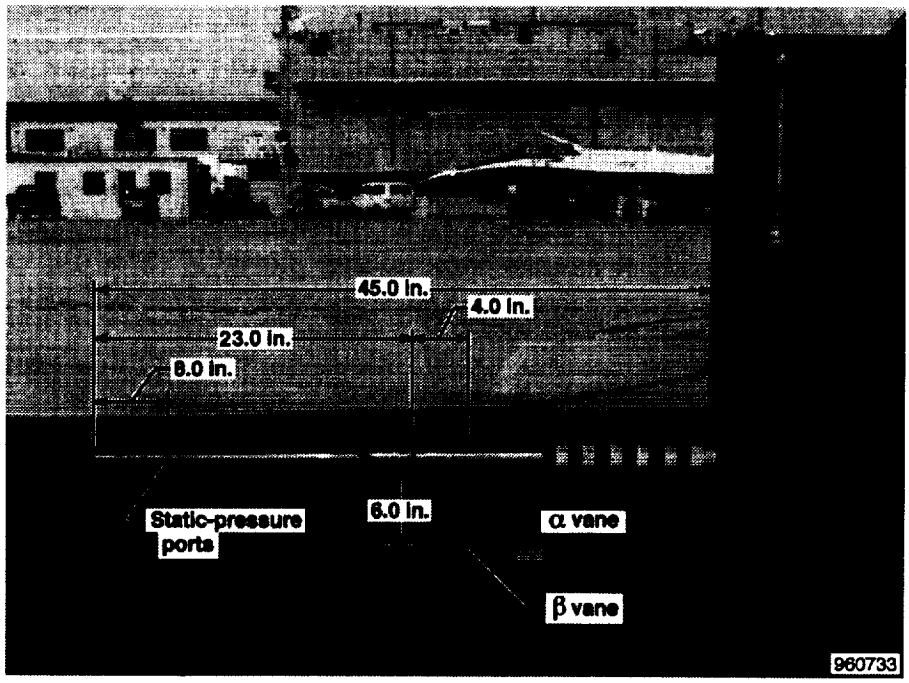

Figure 5. Removable airdata probe on the FTF–II.

Outside wall temperature was measured near the base of the rake at x/c = 0.90 (fig. 4(c)) to assist with boundary-layer calculations. All of these parameters, including an additional canted boundary-layer rake for the right side of the fixture, are available for future flight experiments.

Flight Test Conditions and Data Reduction

Flow quality data were primarily taken at 1-g flight conditions and a matrix of nominal altitudes of 15,000 ft, 30,000 ft, and 45,000 ft in increments of approximately Mach 0.1 throughout the airspeed envelope of the aircraft. Maneuvers such as level accelerations and decelerations and sideslips were conducted in a manner to minimize aircraft fuel consumption while maintaining proper position within the supersonic corridor. For example, at an aircraft indicated altitude, *Hp,* of approximately 45,000 ft, a level acceleration was first performed to a maximum Mach 1.5, followed by a level deceleration and sideslips at specified Mach numbers. Data at greater than Mach 1.5 were obtained by diving from a higher altitude to Mach 2.0 in the most efficient manner possible and then performing a level deceleration at an altitude of 45,000 ft.

Other parameters such as aircraft indicated angle of attack, α_A, and angle of sideslip tend to be limited by aircraft performance. Figure 6 shows that trim α_A slowly decreases and approaches values between 2° and 0° with increasing Mach number for altitudes between 30,000 and 45,000 ft. Further discussion on the FTF–II noseboom angle of attack will be included in the "Flow Environment" section of this report. At subsonic speeds, local angles of sideslip as high as ±8° were attained during most maneuvers except at dynamic pressures greater than 500 lbf/ft^2. The F-15B flight controls limit the rudder deflections at supersonic speeds. Maximum local angles of sideslip as high as ±4° are attainable at approximately Mach 1.3, but flight data indicate that maximum local angles of sideslip are reduced to approximately ±2° at higher Mach numbers.

Future flight experiments may require increased angles of incidence to meet specific research objectives. These increased angles can be achieved through the use of pitchups or sideslips depending on the experiment location and

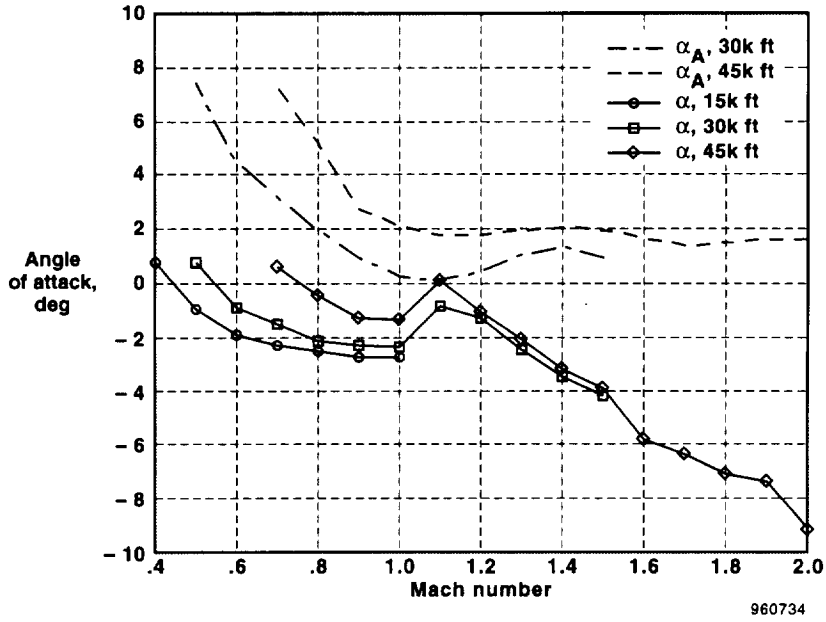

Figure 6. Trim α_A and α as a function of Mach number.

configuration of the FTF–II. Typically, these increased angles of incidence can only be reached at subsonic speeds because of flight control limitations for the F-15B aircraft[10,11] that limit control inputs at supersonic speeds. At Mach 0.5 and an altitude of 30,000 ft, the aircraft can momentarily achieve indicated angles of attack of approximately 20° without significant changes in other flight conditions such as altitude or Mach number. This limitation results in a change in local flow angle on the fixture noseboom of $-1.9° \leq \alpha \leq 4.0°$ and indicates that the flow around the FTF–II is fairly insensitive to aircraft angle of attack. As a result, obtaining local angles of incidence in the pitch axis of the aircraft that are greater than approximately 6° can only be attained by mounting a horizontal surface to the fixture side panel, such as the wedge shown (fig. 7). Larger angles of incidence in the pitch axis can also be

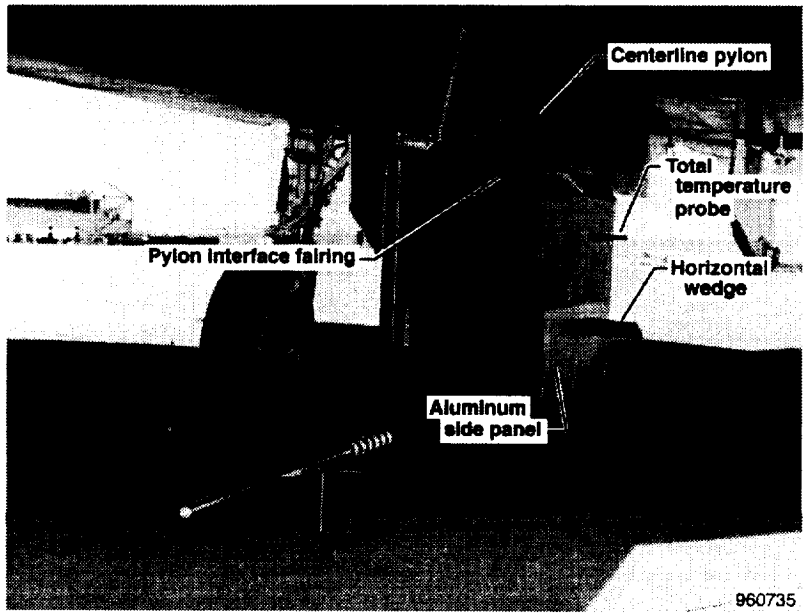

Figure 7. Wedge attached to side panel for shock wave/boundary-layer interaction experiment.

achieved by mounting an object to bottom of the avionics pylon at a predetermined angle of attack. The FTF–II combined with sideslips at subsonic speeds can be used to obtain a range of angles of incidence ±8° in the yaw axis.

The data from all sensors were averaged to minimize errors caused by slight fluctuations in conditions and signal noise. Data from relatively steady maneuvers such as level accelerations and decelerations were averaged over a 1.0-sec interval. More transient maneuvers such as sideslips and pitchups were averaged over a 0.4-sec interval because of rapid changes in flight conditions that would have otherwise been lost in the data reduction process.

RESULTS AND DISCUSSION

Flow conditions at the centerline tank location under the F-15B airplane were characterized by a variety of measurements on the FTF–II. FTF–II noseboom airdata were combined with surface pressure and boundary-layer measurements to survey aerodynamic flow quality. Environmental conditions within the FTF–II were documented as a baseline to assist in the design and testing of avionics and instrumentation for future experiments.

Flow Environment

Flow visualization studies on the FTF–II (fig. 8) indicate that relatively chordwise flow conditions exist over the FTF–II. Flow visualization data are substantiated by measurements of the α (fig. 6). At subsonic speeds (fig. 6), the α ranges from 1° to –3°, depending on the specific flight conditions. At supersonic speeds, downwash over the fixture increases with increasing Mach number to the point where α is approximately –9° at Mach 2.0 (fig. 6). Flow visualization studies (fig. 8) tend to support these results for subsonic and supersonic speeds.

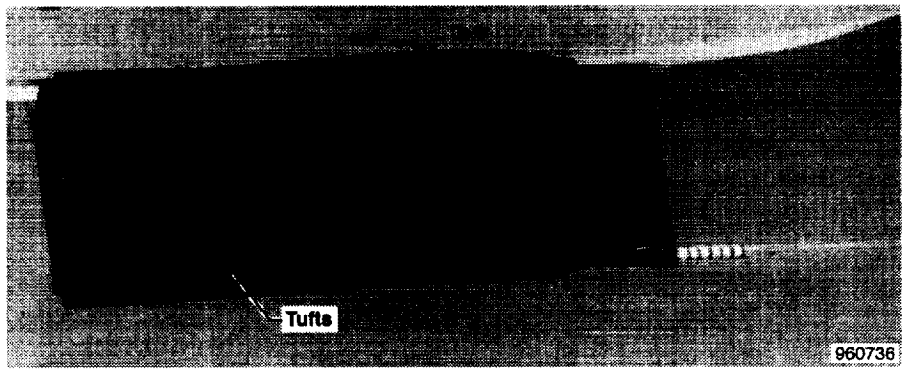

(a) Mach = 0.70, $Hp \approx 45{,}000$ ft, $\beta \approx 0°$.

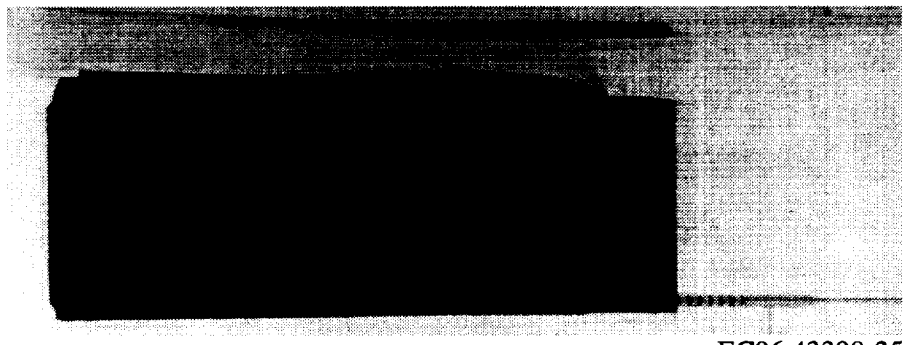

(b) Mach = 1.00, $Hp \approx 45{,}000$ ft, $\beta \approx 0°$.

Figure 8. Flow visualization results obtained in flight, right side with tufts.

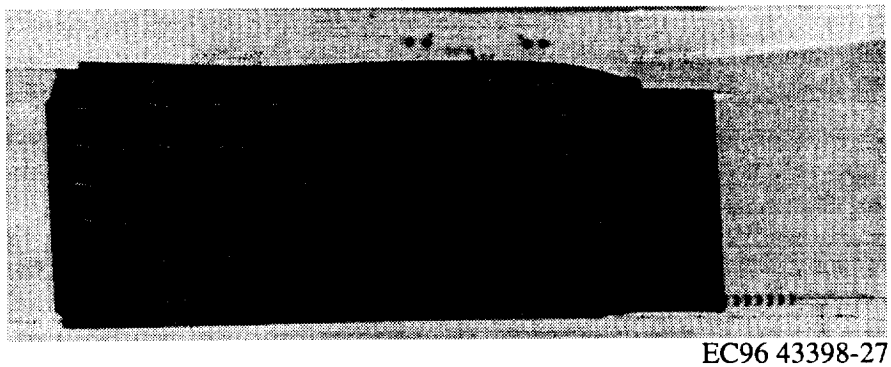

EC96 43398-27

(c) Mach = 1.10, $Hp \approx 45{,}000$ ft, $\beta \approx 0°$.

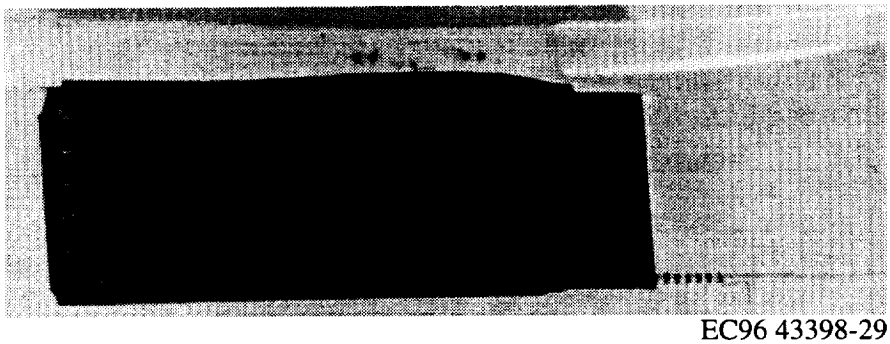

EC96 43398-29

(d) Mach = 1.20, $Hp \approx 45{,}000$ ft, $\beta \approx 0°$.

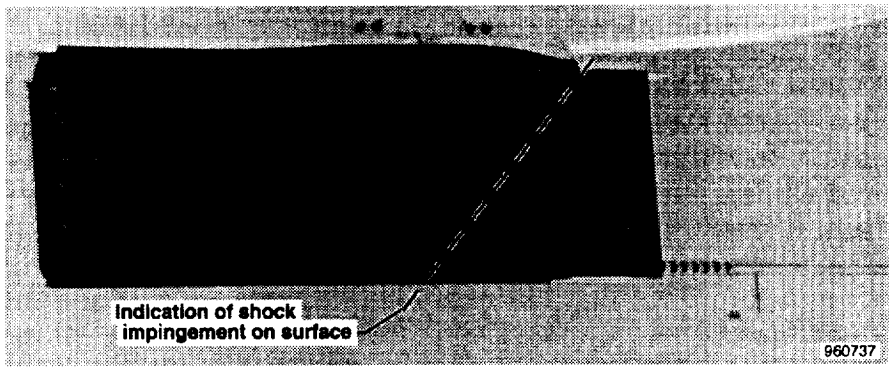

(e) Mach = 1.25, $Hp \approx 45{,}000$ ft, $\beta \approx 0°$.

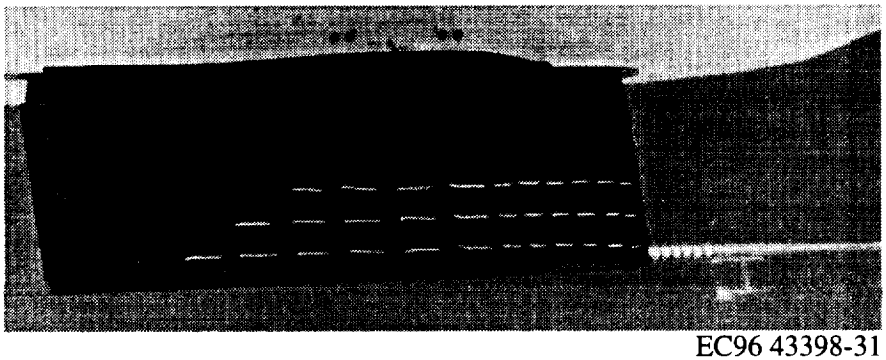

EC96 43398-31

(f) Mach = 1.30, $Hp \approx 45{,}000$ ft, $\beta \approx 0°$.

Figure 8. Concluded.

Although the flow over the FTF–II side panels is generally chordwise, subsequent pressure-distribution data and boundary-layer profiles reveal the effects of shocks from the vicinity of the leading edge of the centerline pylon and fuselage junction. This effect is observed in the discontinuity of the tufts (figs. 8(c) to 8(e)) with the most apparent effects at Mach 1.25. At Mach 1.30 (fig. 8(f)), more chordwise flow conditions reappear. Shocks emanating from the engine inlets were also believed to be the cause for discontinuities in the airdata between Mach 1.0 and 1.4. These anomalies will be highlighted in later sections of this report.

The current F-15B/FTF–II airspeed envelope for airspeeds to a maximum of 600 *KCAS* and Mach 2.0 results in a maximum range in unit Reynolds numbers from 1.0×10^6/ft to 6.0×10^6/ft. As previously reported,[12] the lower limit for the critical Reynolds number for boundary-layer transition for a flat plate at low speeds is approximately 3.2×10^5, although values greater than 1.0×10^6 can occur for very disturbance-free flow. Thus, considering the unit Reynolds number range for the fixture, turbulent flow can be expected to begin naturally within the first foot ($x/c < 0.11$) of the FTF–II nose section at low-speed conditions. Previous FTF–II flight test results[9] using liquid crystals found natural transition locations on the nose section between $x/c = 0.10$ and $x/c = 0.12$, and as far aft as $x/c = 0.16$ at Mach 1.1. Forced transition using artificial surface roughness should be used if a fixed transition point forward of $x/c = 0.10$ is desired for a specific experiment.

Surface Pressure Distributions

Pressure coefficients, C_p, were obtained using the FTF–II free-stream noseboom static pressure, p_∞, and dynamic pressure, q_∞, for reference conditions. Appendix C documents chordwise pressure distributions obtained on the left side of the fixture at $z/b' = 0.16$ (upper), $z/b' = 0.48$ (mid), and $z/b' = 0.86$ (lower) for the entire matrix of flight conditions. The maximum value of the pressure coefficient, $C_{p_{max}}$, at the stagnation point for subsonic flow[13] and behind a normal shock wave for supersonic flow[14] was calculated and included for steady-state maneuvers at an altitude of 45,000 ft for comparison and validation of the FTF–II nose section pressures at $x/c = 0.0$ (table C-3).

Figure 9 shows typical FTF–II chordwise pressure distributions for Mach 0.7 and Mach 1.5. Pressure coefficient values have been offset –0.4 and –0.8 for spanwise locations of $z/b' = 0.48$ and $z/b' = 0.16$, respectively, on the chordwise pressure distribution plots for comparison. As expected, no significant Reynolds number effect at the selected altitudes was observed. Obvious features from the chordwise pressure distributions include the suction peak from the contoured nose section, slight base area effects for $x/c \geq 0.96$ (fig. 9(a)), and the presence of a weak shock from the centerline pylon at $x/c \approx 0.18$ (fig. 9(b)).

Figure 10 shows differences in the chordwise pressure distributions as a function of Mach number. In the subsonic region (fig. 10(a)), chordwise pressure gradients are small between $0.20 \leq x/c \leq 0.90$. At transonic speeds (figs. 10(b) to 10(d)), chordwise pressure distributions increasingly show the effects of compressibility, and the formation of the normal shock from the FTF–II surface is observed at Mach 0.89. Figures 10(b) and 10(c) show the value of the critical pressure coefficient, C_p^*, which corresponds to sonic flow. Figure 11 shows the approximate regions where shock impingement locations were identified on the surface of FTF–II. The normal shock from the FTF–II surface at Mach 0.89 is located slightly upstream of $x/c = 0.21$. From Mach 1.00 to 1.39, the effects of the weak shock from the centerline pylon are seen at the three spanwise locations. At Mach $\geq$ 1.39 (figs. 10 and 11), effects of the shock move aft and weaken. A more detailed analysis of this region of weak shock interactions would require additional instrumentation.

Smaller chordwise pressure gradients are again present for Mach $\geq$ 1.60 (figs. 10(f) to 10(h)). The slight rise in the surface pressure at $z/b' = 0.86$ and $x/c = 0.90$ at supersonic speeds is believed to be caused by the presence of the boundary-layer rake near this location and the resulting rise in local static pressure. The influence of the rake on local flow is typical of a local disturbance that may occur if external hardware is mounted on a side panel of the FTF–II for future experiments.

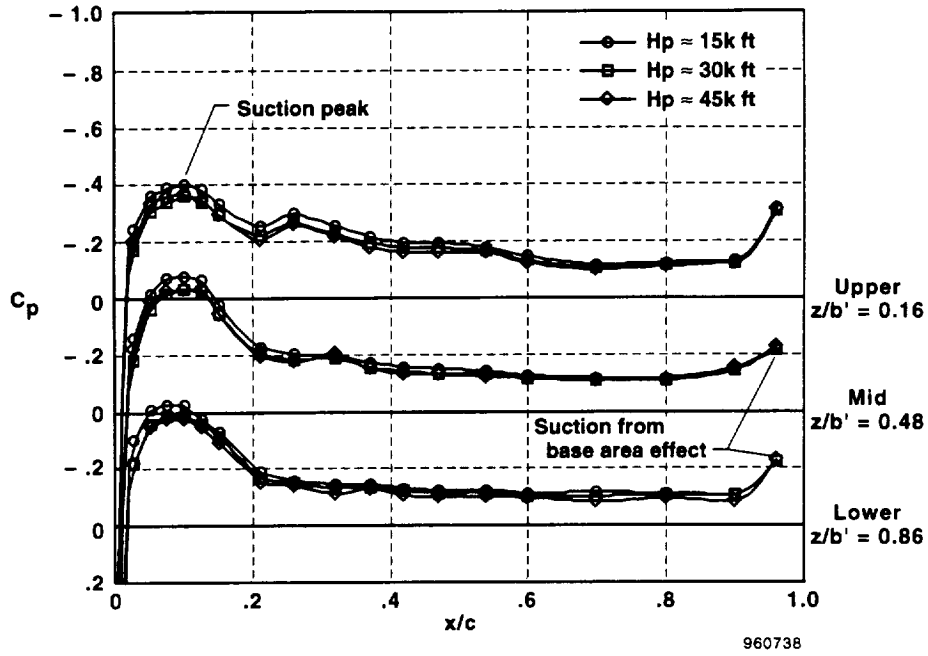

(a) Mach = 0.7.

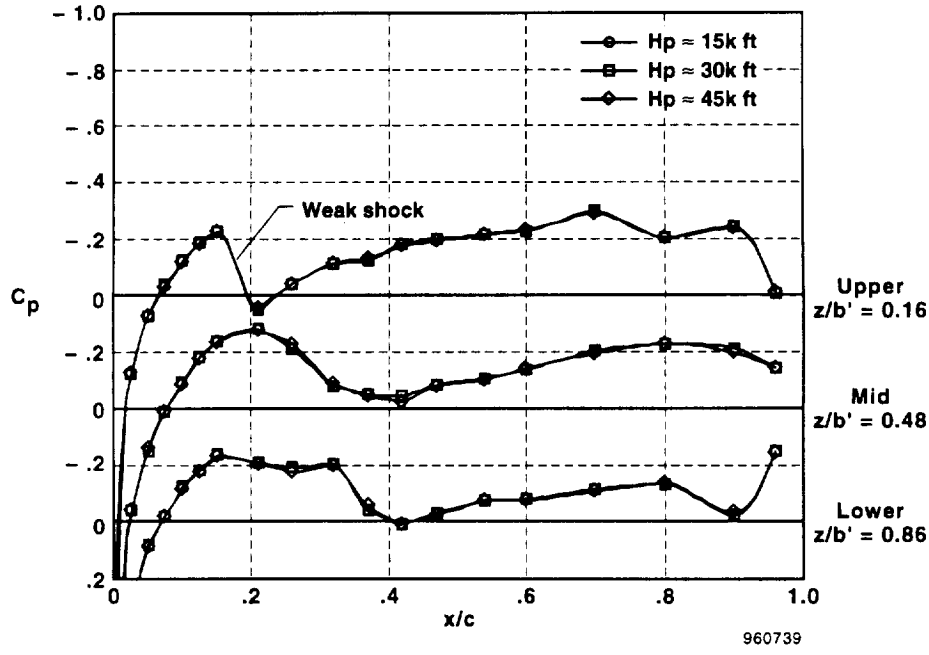

(b) Mach = 1.5.

Figure 9. Chordwise pressure distributions obtained in flight at specified Mach numbers and altitude.

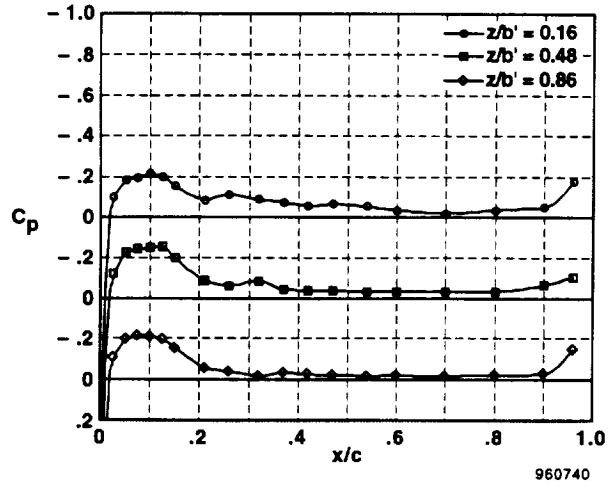

(a) Mach = 0.39, $Hp \approx$ 15,000 ft.

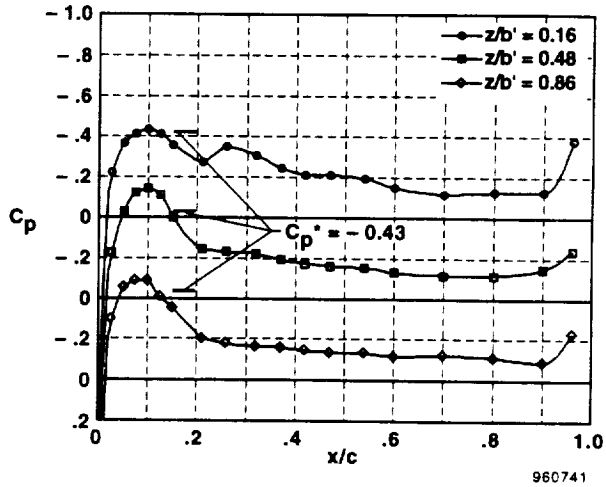

(b) Mach = 0.80, $Hp \approx$ 15,000 ft.

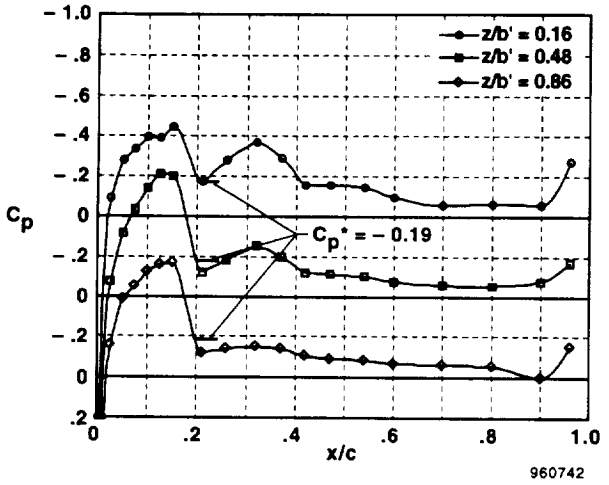

(c) Mach = 0.89, $Hp \approx$ 30,000 ft.

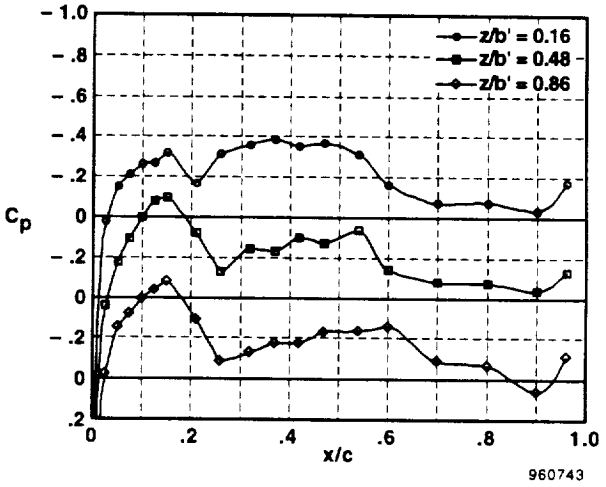

(d) Mach = 1.00, $Hp \approx$ 30,000 ft.

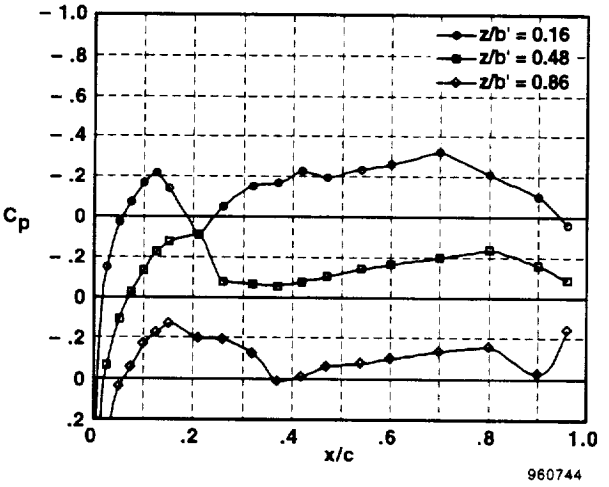

(e) Mach = 1.39, $Hp \approx$ 30,000 ft.

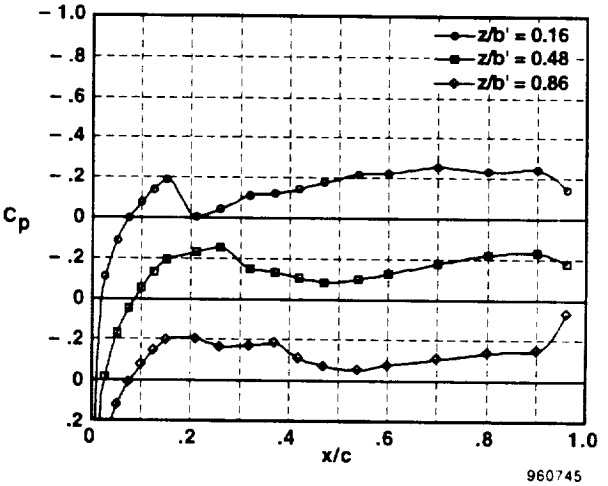

(f) Mach = 1.60, $Hp \approx$ 45,000 ft.

Figure 10. Chordwise pressure distributions obtained in flight at specified Mach numbers.

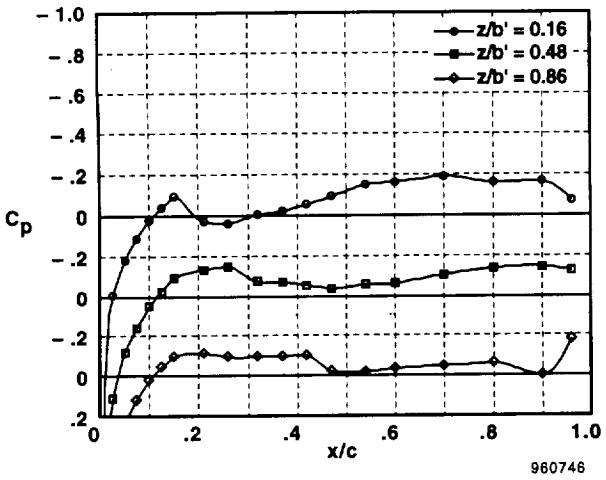

(g) Mach = 1.80, $Hp \approx 45{,}000$ ft.

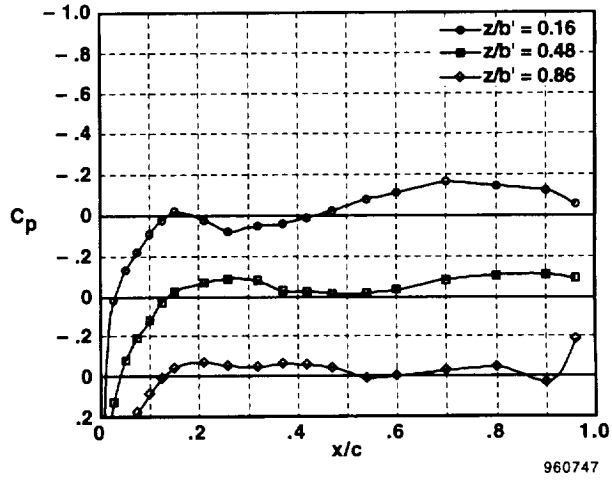

(h) Mach = 2.00, $Hp \approx 45{,}000$ ft.

Figure 10. Concluded.

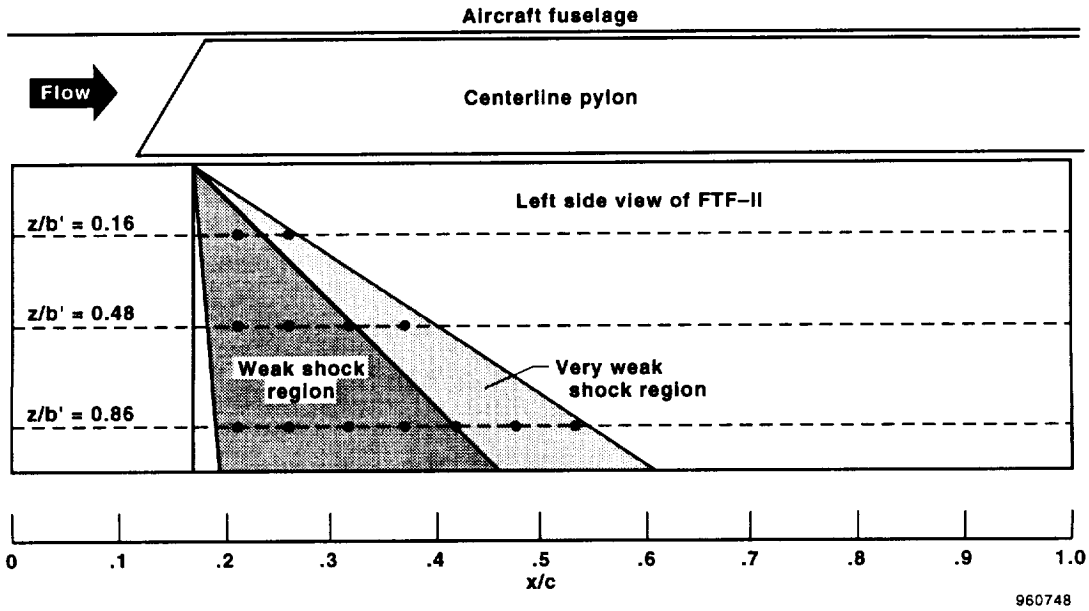

Figure 11. Approximate regions of shock impingement on the surface of the FTF–II derived from flight data.

Figure 12 shows chordwise pressure distributions at approximately Mach 0.54 are essentially insensitive to changes in α from –1.85° to 4.05°, as expected. Figures 13 and 14 show differences in the chordwise pressure distributions as a function of sideslip. At Mach 0.52 (fig. 13), the most significant feature of the chordwise pressure distributions is the suction peak followed by recompression on the leeward side of the fixture. As β approaches –8.0° (windward side), pressure coefficient values approach zero for $x/c \geq 0.20$. Figure 14 shows pressure distributions for Mach 1.28 as β varies approximately ±3.6°. Spanwise effects as a function of β appear to be minor.

Because the differences in the chordwise pressure distributions for the three spanwise locations are relatively minor, the spanwise location of $z/b' = 0.48$ was selected to present chordwise pressure distributions as a function of Mach number and sideslip. Pressure coefficient values (figs. 15(a) to 15(c)) have been offset –0.8, –0.6, –0.4, and –0.2 for β of 8.0°, 4.0°, 0°, and –4.0°, respectively. Figure 15(d) shows pressure coefficient values that have been

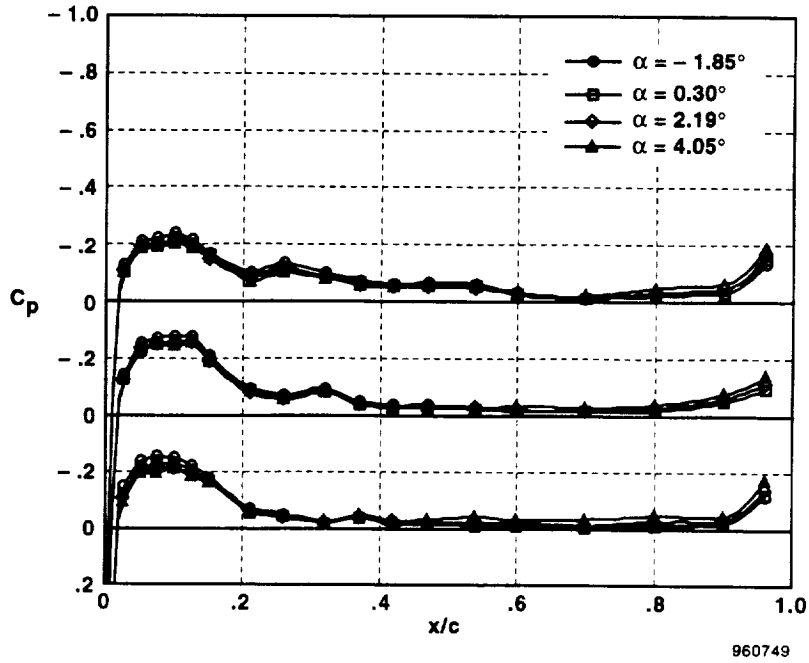

Figure 12. Chordwise pressure distributions obtained in flight at specified FTF–II angles of attack; Mach ≈ 0.54, $\beta \approx 0°$, $Hp \approx 30{,}000$ ft.

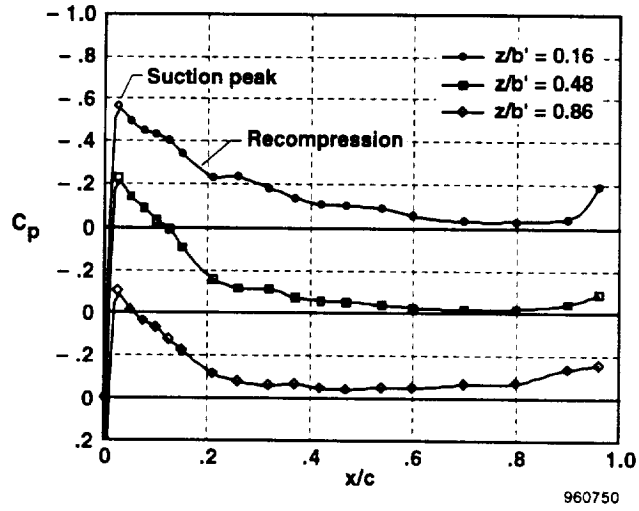

(a) $\beta = 8.04°$, leeward.

Figure 13. Chordwise pressure distributions obtained in flight at specified angles of sideslip; Mach = 0.52, $Hp \approx 15{,}000$ ft.

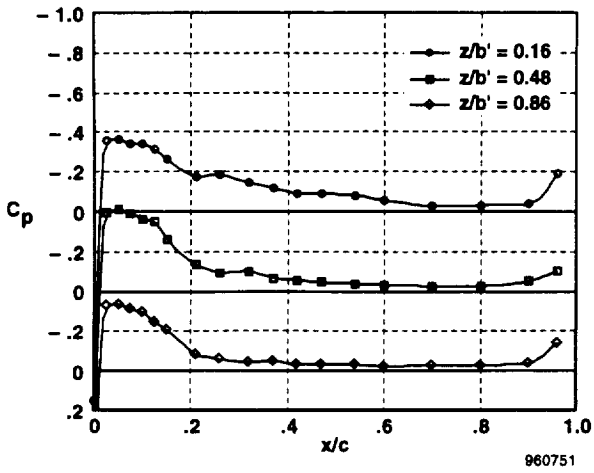

(b) β = 3.95°, leeward.

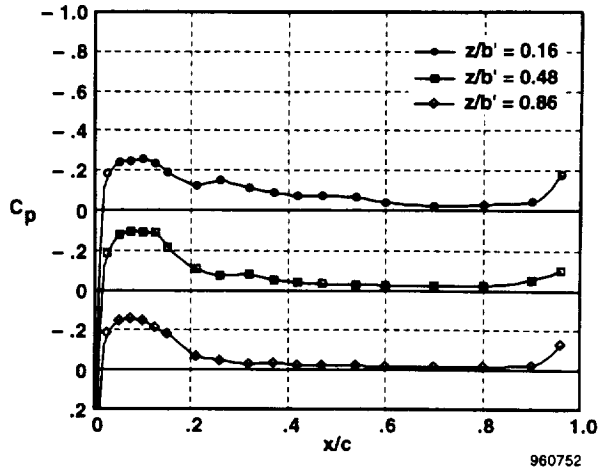

(c) β = 0.00°.

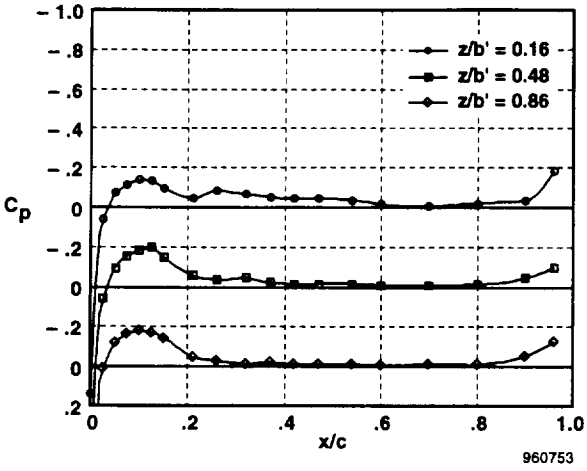

(d) β = –3.98°, windward.

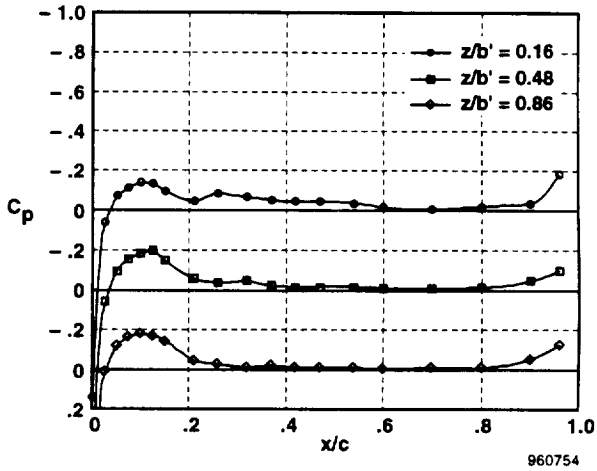

(e) β = –8.00°, windward.

Figure 13. Concluded.

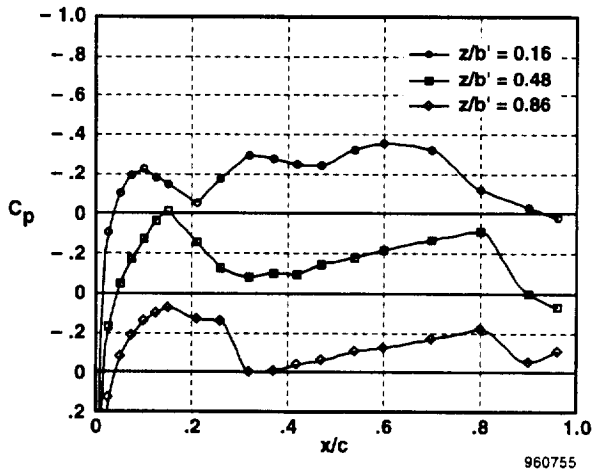

(a) β = 3.57°, leeward.

Figure 14. Chordwise pressure distributions obtained in flight at specified angles of sideslip; Mach = 1.28, *Hp* ≈ 45,000 ft.

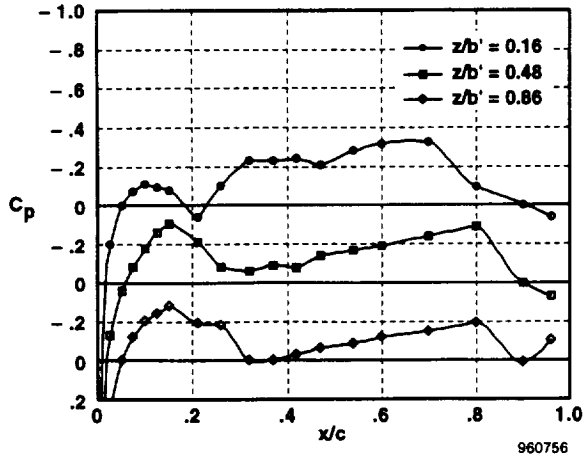

(b) β = 1.93°, leeward.

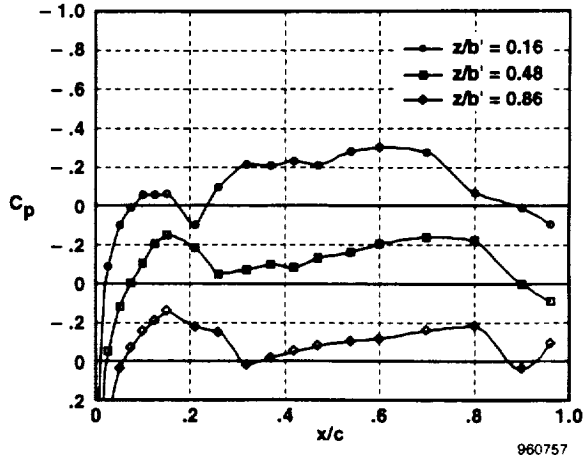

(c) β = –0.07°.

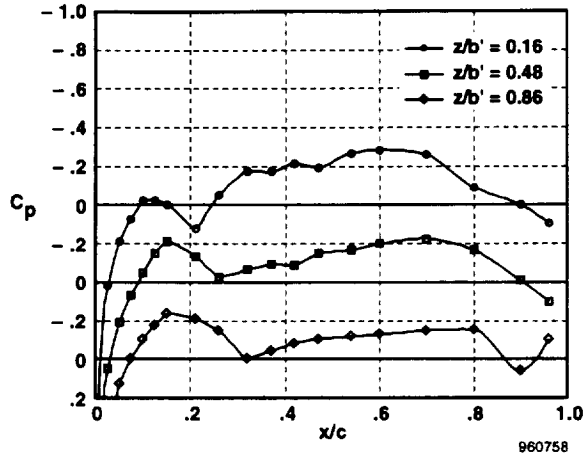

(d) β = –2.02°, windward.

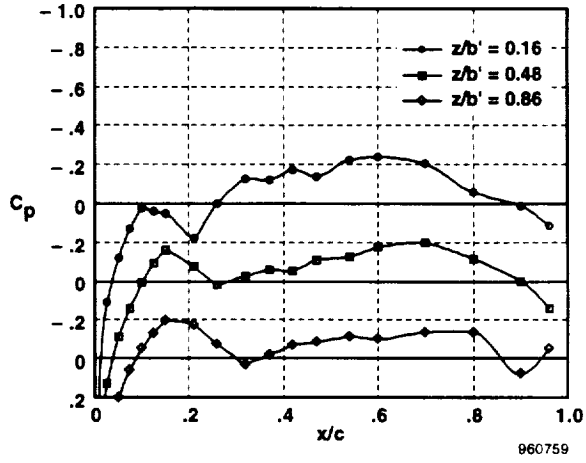

(e) β = –3.59°, windward.

Figure 14. Concluded.

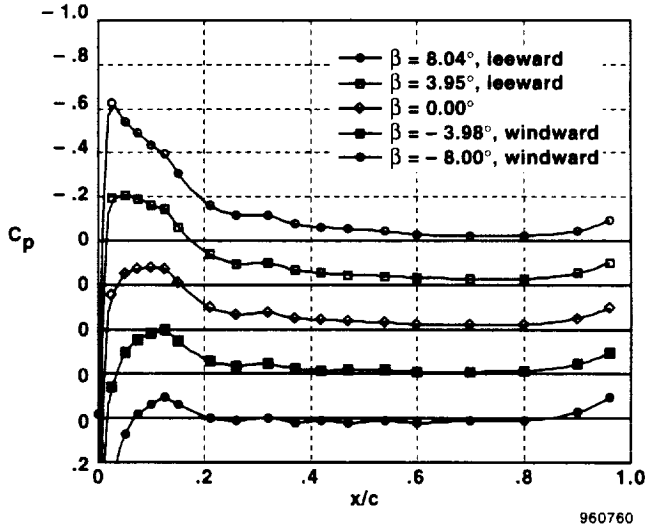

(a) Mach = 0.52, *Hp* ≈ 15,000 ft.

Figure 15. Chordwise pressure distributions obtained in flight at specified Mach numbers and angles of sideslip; *z/b'* = 0.48.

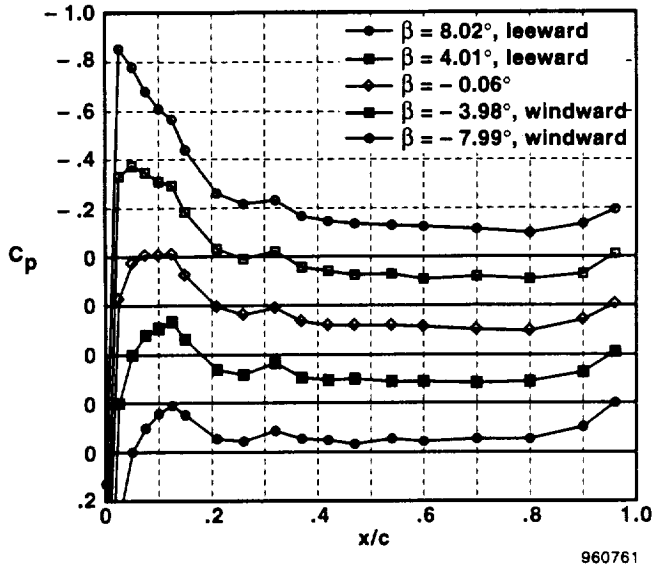

(b) Mach = 0.70, $Hp \approx 45{,}000$ ft.

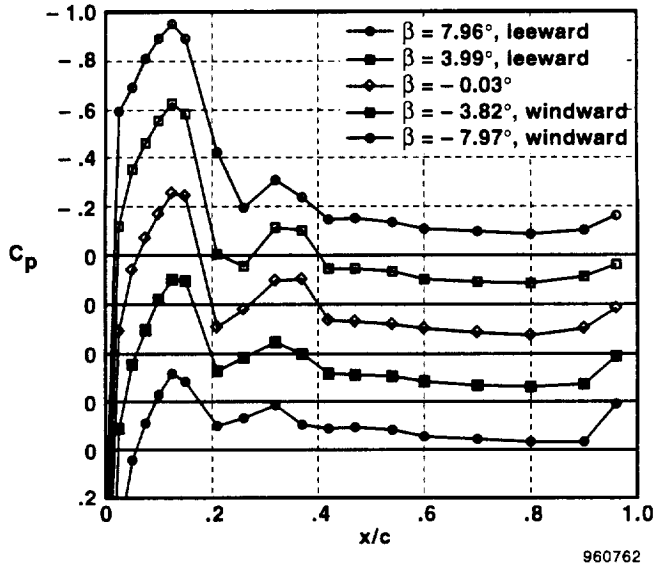

(c) Mach = 0.89, $Hp \approx 45{,}000$ ft.

Figure 15. Continued.

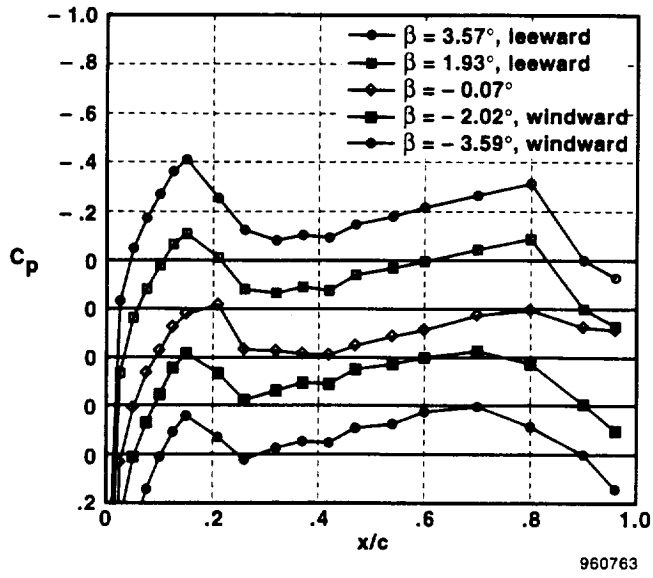

(d) Mach = 1.28, $Hp \approx 45{,}000$ ft.

Figure 15. Concluded.

offset –0.8, –0.6, –0.4, and –0.2 for β of 3.6°, 2.0°, 0°, and –2.0°, respectively. Again, the most significant feature of the chordwise pressure distributions as a function of Mach and β are the suction peak followed by recompression on the leeward side of the fixture. Another interesting feature is the change toward higher pressures near the aft region of the FTF–II at Mach 1.28 (fig. 15(d)).

Boundary-Layer Measurements

Because of the influence of the boundary-layer rake on the local static pressure at $z/b' = 0.86$ and $x/c = 0.90$, velocity profiles (u/U_r) were calculated using a reference static pressure (p_w) orifice located at the same chord location and at $z/b' = 0.48$. Appendix D shows boundary-layer data obtained on the left side of the fixture tabulated for the entire matrix of flight conditions. Local flow qualities such as the maximum local Mach number from the rake (M_r), total airstream temperature (T_f), local wall temperature (T_w), and p_w, have been included for steady-state maneuvers to aid in planning experiments that may require further analysis of the boundary-layer. Reynolds numbers at the rake (based on a rake location of $x/c = 0.90$) ranged from 8.02×10^6 to 36.9×10^6, depending on specific flight conditions. For this report, boundary-layer thickness, δ, is defined as the distance from the wall where velocity is 99 percent of the maximum local free-stream velocity.[12]

The reference Mach number for the boundary-layer data is the M_r obtained from the outer probes of the rake that are outside the boundary layer. Figure 16 shows the relationship for the M_r to the free-stream Mach number obtained from the FTF–II noseboom, M_∞. As figure 16 shows, little effect from altitude or Reynolds number exists on the relationship of M_r/M_∞. The M_r shows a slight increase over the M_∞ at subsonic speeds. For $M_\infty \approx 1.0$ to 1.25, the M_r is slightly less than the M_∞ and then appears to increase to $\Delta M \approx 0.2$ at greater than $M_\infty \approx 1.4$.

Figures 17 and 18 show typical FTF–II boundary-layer profiles. The losses in the boundary layer at the respective altitudes are mostly consistent with the expected Reynolds number effect for the profiles shown (fig. 17). In general, large boundary-layer losses are observed at the low Reynolds numbers that occur at the high altitudes. Because the boundary layer was not tripped at a fixed chord location, differences in the various profiles may have also resulted from small differences in β and transition location effects.

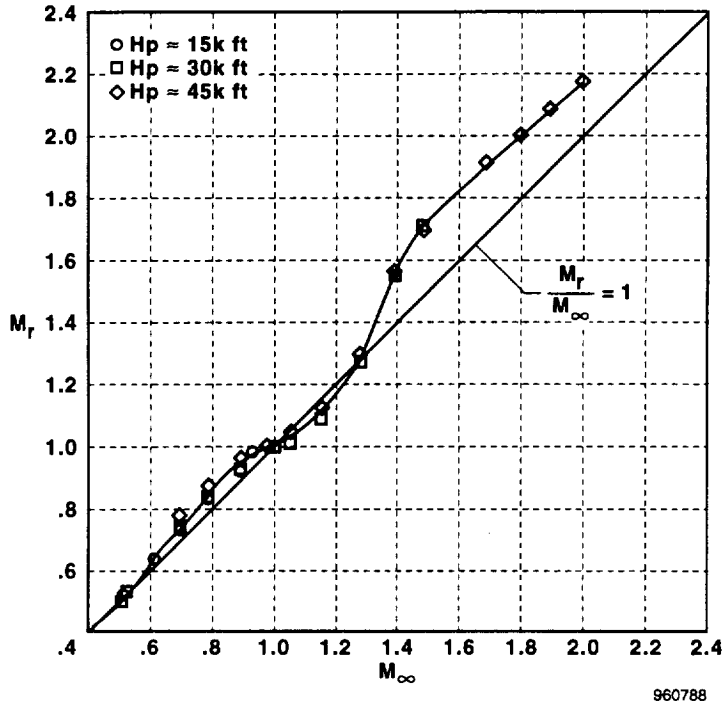

Figure 16. In-flight relationship of M_r with M_∞, outside the boundary layer, $x/c = 0.90$.

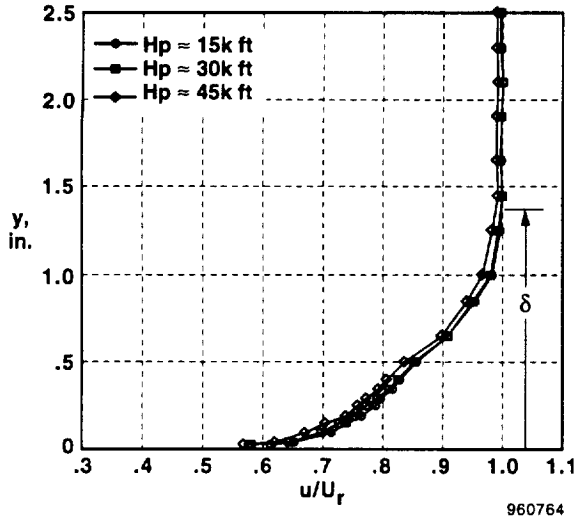

(a) Mach ≈ 0.7.

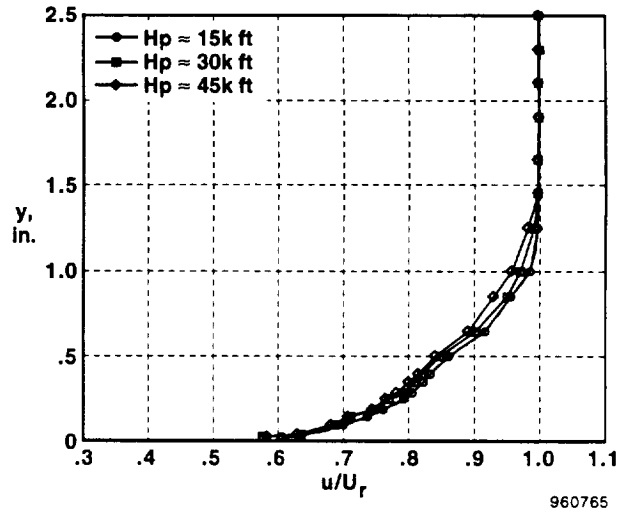

(b) Mach ≈ 0.9.

Figure 17. Boundary-layer profiles obtained in flight at specified Mach numbers and altitude.

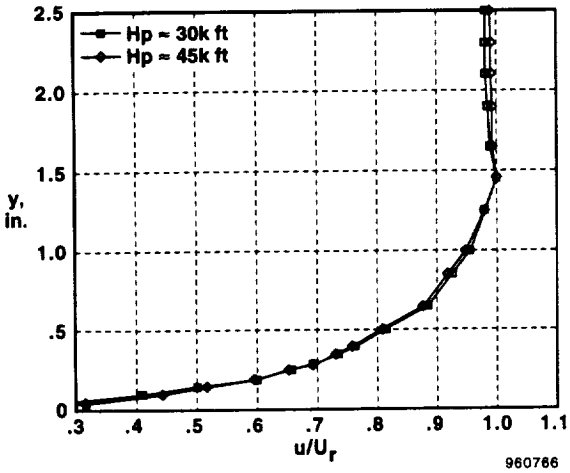

(c) Mach ≈ 1.4.

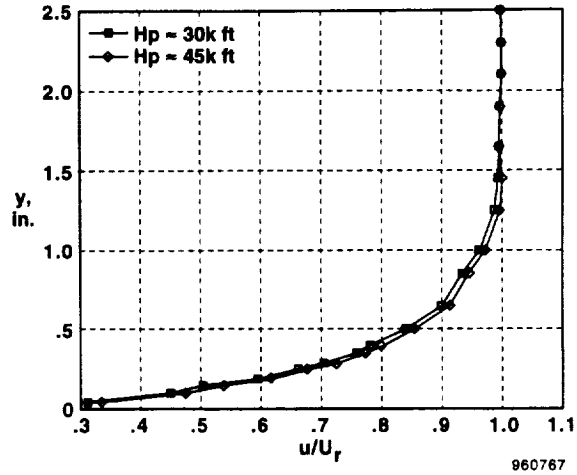

(d) Mach ≈ 1.5.

Figure 17. Concluded.

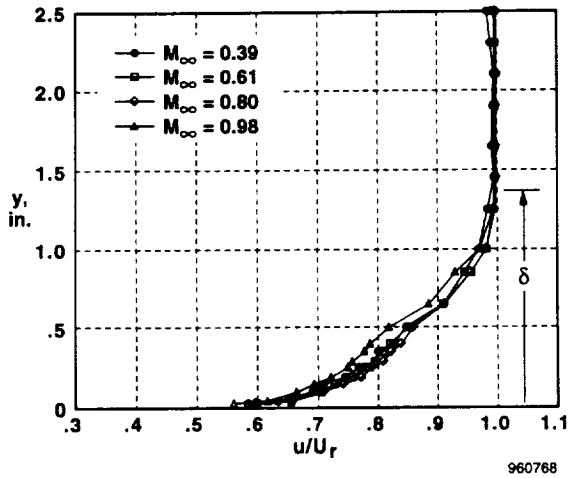

(a) *Hp* ≈ 15,000 ft.

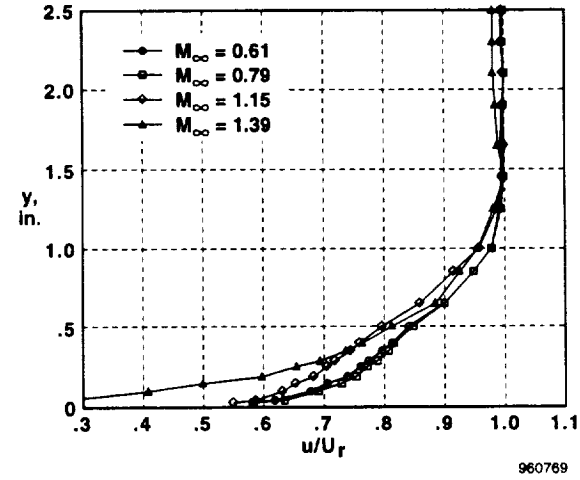

(b) *Hp* ≈ 30,000 ft.

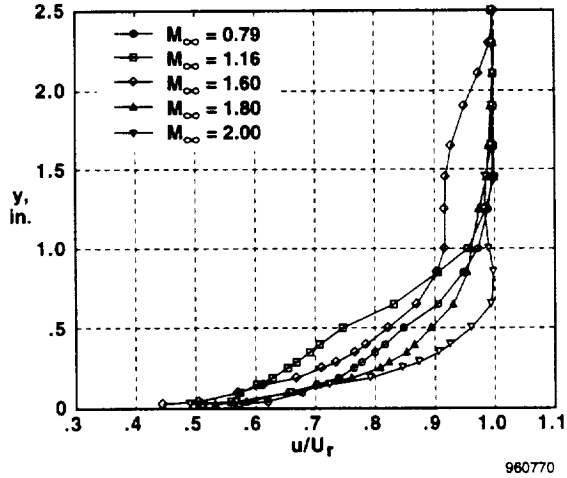

(c) *Hp* ≈ 45,000 ft.

Figure 18. Boundary-layer profiles obtained in flight at specified altitude and Mach numbers.

Figure 18 shows boundary-layer profiles at various Mach numbers for the three selected altitudes. At each altitude, the profiles for Mach ≤ 0.8 are generally similar with no significant features beyond mild inflections. The profile at Mach 0.98 (fig. 18(a)) shows a more exaggerated inflection. The remaining profiles at supersonic conditions are quite different from those observed at the low Mach numbers. The presence of upstream shocks, located uniquely for each Mach number, appear to impose unique upstream conditions on the boundary layer at the specific Mach number. In addition, reinspection of surface pressure-distribution data (figs. 9 and 10) also shows the general presence of an adverse pressure gradient in the rake location during supersonic conditions. Future boundary-layer measurements forward of $x/c = 0.90$ should be considered to identify and avoid any possible effects from an adverse pressure gradient.

In general, boundary-layer thickness ranged from 1.25 in. to 1.45 in. with a slight increase at the supersonic Mach numbers (figs. 18(a) and (b)). As an approximation, calculation of boundary-layer thickness for a flat plate with a turbulent boundary layer[12] using the origin of turbulent flow at $x/c = 0.12$[9] predicts a boundary-layer thickness of 1.28 in. to 1.49 in. for the range of flight test Reynolds numbers. This prediction shows general agreement with flight results. As a result, the following equation may be used to estimate boundary-layer thickness[12] for future FTF–II experiments in a similar configuration with natural transition:

$$\delta/l = 0.37(\mathrm{Re}_l)^{-1/5}$$

where $l = x - \Delta x$, in.

and x = distance from leading edge to test location, in.

and Δx = 12.84 in.

A more appropriate estimation for forced transition would be to set Δx as the location of the forced transition aft of the FTF–II leading edge.

Figures 19 and 20 show boundary-layer profiles at various angles of attack and sideslip, respectively. Changes in the boundary layer were observed as a function of changes in α (fig. 19). Large changes in the boundary layer, as noted by the inflection in the boundary-layer profile, did not occur until $\alpha = 4.05°$, which corresponds to $\alpha_A \approx 20°$.

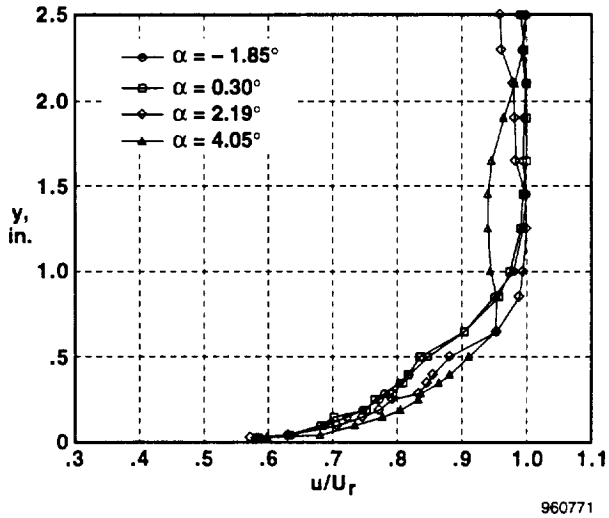

Figure 19. Boundary-layer profiles obtained in flight at specified FTF–II angles of attack; Mach ≈ 0.54, $\beta \approx 0°$, $Hp \approx 30{,}000$ ft.

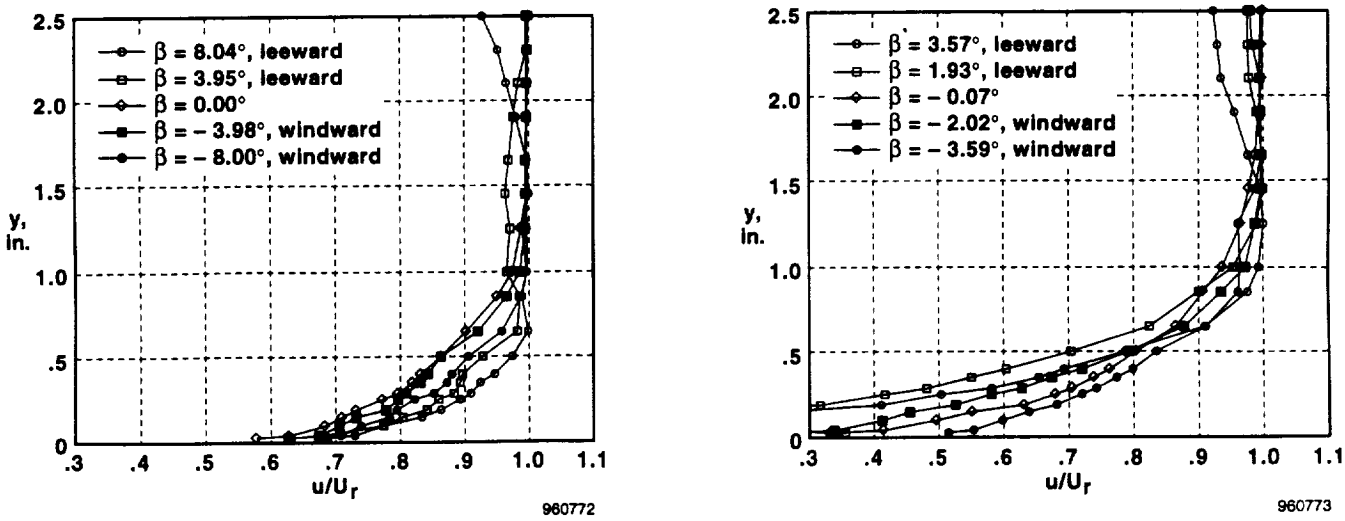

(a) Mach = 0.52, $Hp \approx 15{,}000$ ft.

(b) Mach = 1.28, $Hp \approx 45{,}000$ ft.

Figure 20. Boundary-layer profiles obtained in flight at specified angles of sideslip.

This observation is a useful finding for experiments that plan to utilize a horizontal surface mounted to a fixture side panel that may require slight changes in α.

Figure 20 shows boundary-layer profiles at sideslip conditions for subsonic and supersonic Mach numbers. At Mach 0.52 (fig. 20(a)), the most distorted boundary-layer profiles are obtained for leeward flow at the sideslip angles where $\beta \geq 3.95°$. At Mach 1.28 (fig. 20(b)), leeward flow also produces the most distorted profiles at $\beta = 3.57°$.

Internal Environment

To characterize the internal environment within the FTF–II, bay temperatures were obtained on multiple flights for a wide range of initial temperatures during preflight and for a variety of flight conditions to determine typical and extreme temperatures. Acceleration data were also obtained to determine in-flight acceleration loads within the FTF–II.

Bay Temperatures

For simplicity, the FTF–II has no active environmental controls to control internal temperature. As a result, bay temperatures were monitored during all ground and flight testing of the FTF–II to document typical and worst-case bay temperatures. Temperatures for bays A2, A3, T1, T2, T3, and T4 (fig. 4(a)) followed expected trends but were dependent on ground and flight conditions. As expected, bay temperatures during pre- and post-flights were primarily affected by the ambient air temperature. In-flight bay temperatures were primarily affected by the ambient air temperature at altitude and the duration of testing at altitude. Aerodynamic heating effects at the higher Mach numbers had little impact on temperatures within the fixture because of the limited duration of testing at these conditions. Heating produced by the avionics or instrumentation within each bay affected individual bay temperatures, but the trends in bay temperatures were consistent and easy to estimate for ground and flight operations.

Figure 21 shows bay temperatures for a typical flight profile with an ambient air temperature of 70 °F prior to the flight. Bay temperatures ranged from 5 to 35 °F higher than the ambient air temperature, depending on the heating produced by the equipment in a specific bay. After aircraft takeoff, temperatures began to drop as expected. The

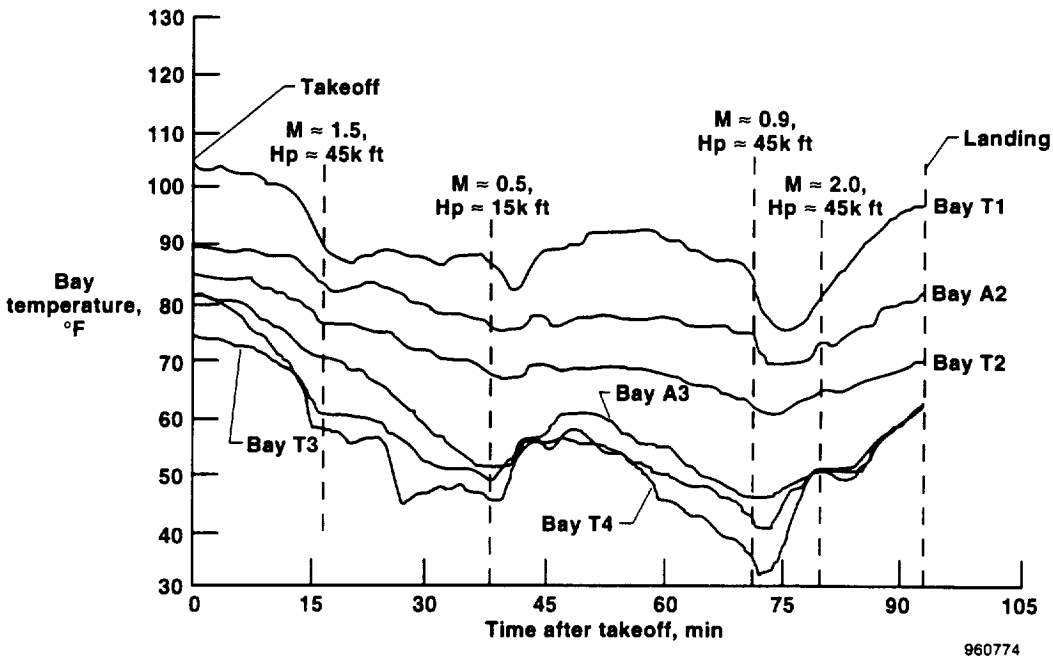

Figure 21. FTF–II bay temperatures obtained during a typical flight profile.

lowest observed bay temperature of approximately 30 °F occurred in bay T4 after approximately 70 min of flight testing at altitudes between 15,000 ft and 45,000 ft. Temperatures began to increase with a return to low altitudes prior to landing at the completion of the flight. From these data, the maximum expected range of internal temperatures within the FTF–II is 30–105 °F. Because ambient air temperatures at NASA Dryden can vary ±40 °F, projected worst-case internal temperatures within the FTF–II would be –10 °F in-flight to 145 °F during ground operations. More extreme temperatures could exist, depending on a wide variety of experiment variables. Experiments with temperature sensitive equipment are advised to use thermal control systems or monitor bay temperatures near the location of the flight experiment.

Vibration Data

High-frequency data from piezoelectric accelerometers were obtained to document local three-axis accelerations inside the FTF–II. Accelerometer data were recorded on tape at various flight conditions, low-pass filtered at 2000 Hz, and digitized at 8192 samples/sec for further analysis. Short time segments (1 sec) of relatively constant flight conditions were used to calculate root mean square (rms) magnitudes and power spectral density (PSD) functions. Each PSD is an average of 30 overlapped records spanning a given 1-sec interval.

During the analysis process, y-axis data were determined to be unreliable. As a result, only x- and z-axis data have been summarized in this report. Figure 22 shows acceleration and PSD results from typical flight maneuvers for the x and z axis. At Mach 0.70 (fig. 22(a)), g levels tend to increase with β. At $\beta \approx -5°$, maximum g_{rms} is approximately 6.0 and 3.5 for the x and z axes, respectively. The corresponding PSD plot indicates that most the accelerations occur as random input at greater than 200 Hz. For clarity, only the maximum and minimum values for a given PSD set are plotted. Data from an acceleration/deceleration between Mach 1.0 and 1.5 and from Mach 1.9 to 2.0 show similar g_{rms} levels and spectral content (fig. 22(b)). Figure 22(b) also shows that g levels tend to increase with Mach number. At Mach 2.0, maximum g_{rms} is approximately 6.0 and 3.0 for the x axis and z axis, respectively.

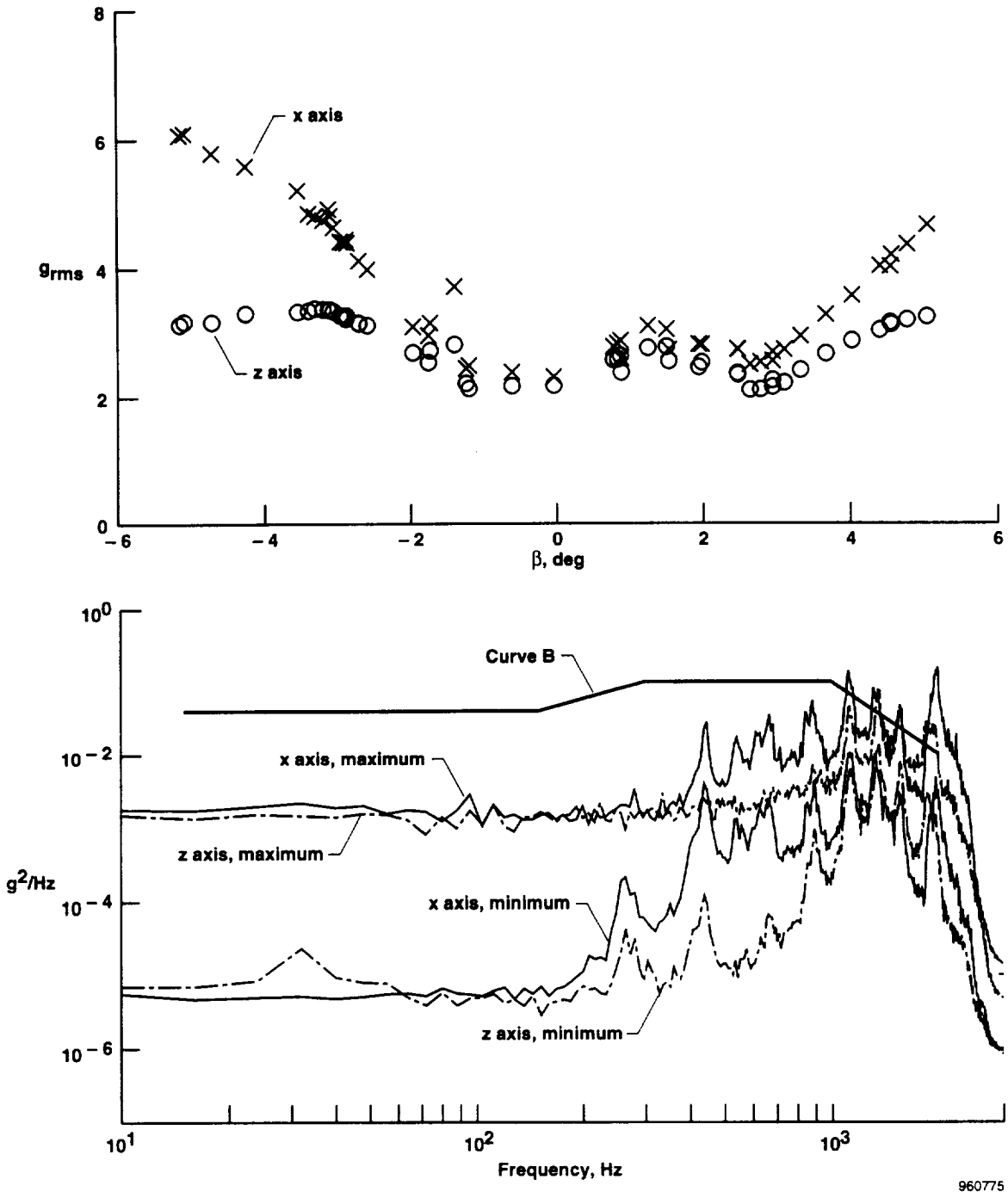

(a) Sideslip, Mach = 0.70, $Hp \approx 15{,}000$ ft.

Figure 22. FTF–II accelerometer data obtained in flight.

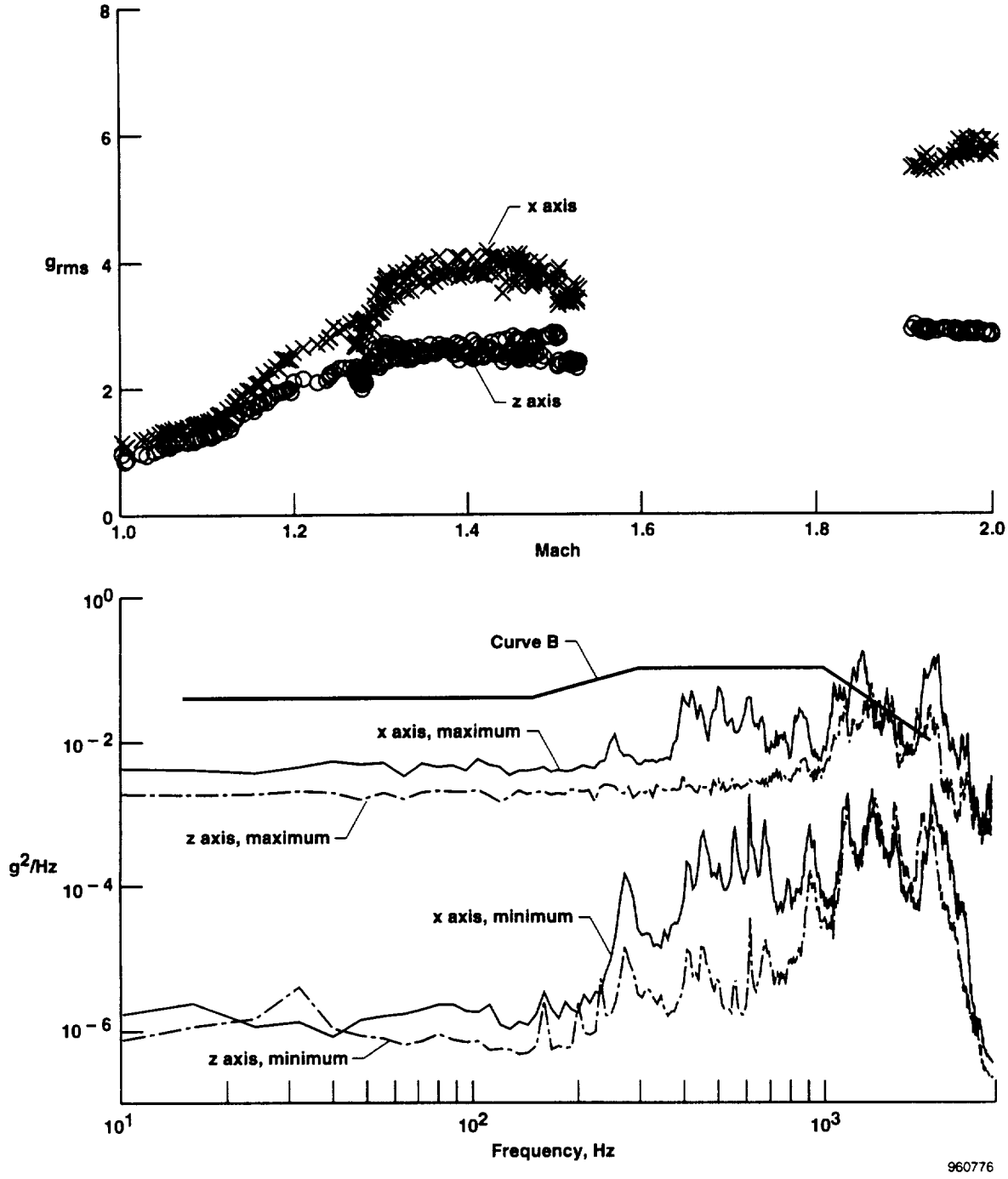

(b) Acceleration/deceleration, $Hp \approx 45{,}000$ ft, $\beta \approx 0°$.

Figure 22. Concluded.

The significant result from analysis of the accelerometer data (x and z axis) is that $g_{rms} \leq 6.0$ for most flight conditions within the operational envelope of the F-15B/FTF–II. Further details on how the flight data can be related to FTF–II vibration test requirements, such as Curve B (fig. 22), are included in the next section of this paper. A more comprehensive study, including y-axis data, of FTF–II local accelerations must be completed before a reduction in the FTF–II vibration test requirements can be considered for all experiment-related hardware.

Designing Fixture Experiments

Understanding the aerodynamics and internal environment of the FTF–II is important but is only a contributing factor in the development of a flight experiment. Successful design of an FTF–II experiment will require a basic understanding of established NASA Dryden policies and guidelines as well as alternate FTF–II configurations that can be achieved to meet specific experiment requirements. This section serves as a guide to assist in the development of future experiments on the FTF–II. Additional information enclosed in the appendices has been included to assist with more detailed analyses by project personnel, if required.

Established Policies and Guidelines

NASA Dryden requires flight projects such as the F-15B/FTF–II to follow established policies and guidelines to help achieve efficient flight operations without compromising safety. The most relevant NASA Dryden documents for developing flight experiments on the FTF–II are the *Basic Operations Manual,*[*] *Procedures for Objectives & Research Requirements Documents,*[†] and *Process Specification Manual.*[‡] All of these documents are available to NASA Dryden personnel, and specific requests can be accommodated. The *Basic Operations Manual* outlines the basic established policies for NASA Dryden flight projects and provides some guidelines to assist with implementing these policies. The *Basic Operations Manual* reviews policies on issues such as risk management, system safety, quality assurance, project plans, configuration management, flight preparation, and flight readiness and review processes at NASA Dryden.

Much of the input into project plans is derived from information that is submitted in the form of an Objectives and Research Document (ORD). An ORD is the link between the technical objective and the proposed experiment requirements. All F-15B/FTF–II experiments require that an ORD be submitted to the project for evaluation and approval. As a minimum, this ORD should include[16] an experiment title, an introduction, an objective, the test scope and approach, specific requirements, and the appropriate approvals. Early development and approval of an ORD ensures that specific experiment requirements are defined and reasonable flight objectives can be achieved in a safe and timely manner by the project.

Another key document for compliance in the development of a flight experiment is the NASA Dryden *Process Specification Manual.* The purpose of this document is to provide specification for the acceptance of avionics, instrumentation, or experimental hardware mounted internally or externally on the FTF–II. The primary specification sections of interest for potential flight experiments are "Section 00 - Operations" and "Section 21 - Testing." For testing, because the F-15B airplane is a jet aircraft and the FTF–II is installed at the centerline pylon location, all FTF–II hardware must meet the vibration test requirements for Category II aircraft Curve B. Because the FTF–II is not a temperature-controlled environment, all electronics should be tested for operation from –65 to 160 °F and to

[*]National Aeronautics and Space Administration Dryden Flight Research Center *Basic Operations Manual*, X-1.000, Rev. 5, Feb. 1995.

[†]Bauer, Carol A., *Procedures for Objectives & Research Requirements Documents (ORDS)*, Dryden Flight Research Center, Rev. 12/87, Dec. 1987.

[‡]NASA Dryden Flight Research Center, *Process Specification Manual*, Rev. 5/95, May 1995.

an absolute pressure equivalent of 60,000 ft, which is the altitude limit of the F-15B aircraft. Vibration tests on all hardware should be performed using a random vibration test curve equivalent to the 12.2 g^2/Hz, to a maximum 2,000 Hz (fig. 22). These test specifications are the result of many years of flight test experience and should be followed whenever possible to ensure flight safety, avoid aircraft operating restrictions, and ensure a successful flight experiment.

Alternate Fixture Configurations

Past experience with the F-104 FTF has shown the value of a versatile fixture where configuration changes can be accomplished without major structural changes to the fixture. A major design goal during the development of the FTF–II was to maintain the maximum practical configuration versatility. As discussed previously, the primary FTF–II shape (fig. 4) can be modified to satisfy the requirements for a variety of flight experiments. The lower 13 in. of the FTF–II, the vertical test article, can be replaced by aerodynamic shapes that may provide a better match to specific experiment requirements. Other configuration changes (fig. 4) can range from alternate side panels to an alternate nose section for the avionics pylon and test article.

Several "standard" alternate configuration changes have already been developed for the FTF–II. Spare nose section test panels and test article aft left side panels have been fabricated for future experiments. An aft fairing that closely matches the nose section contour (fig. 23) was installed after obtaining the pressure data presented in this paper in order to improve the aft region flow quality, reduce the base drag of the FTF–II, and reduce the resulting base area effects that cause the pressure gradients observed in the pressure data at $x/c \geq 0.90$. An example of a significant configuration change to the FTF–II was for the thermal protection systems durability program (fig. 24). For this program, an alternate nose section was installed to contain tile specimens, and the vertical test article was replaced by a particle measurement probe.

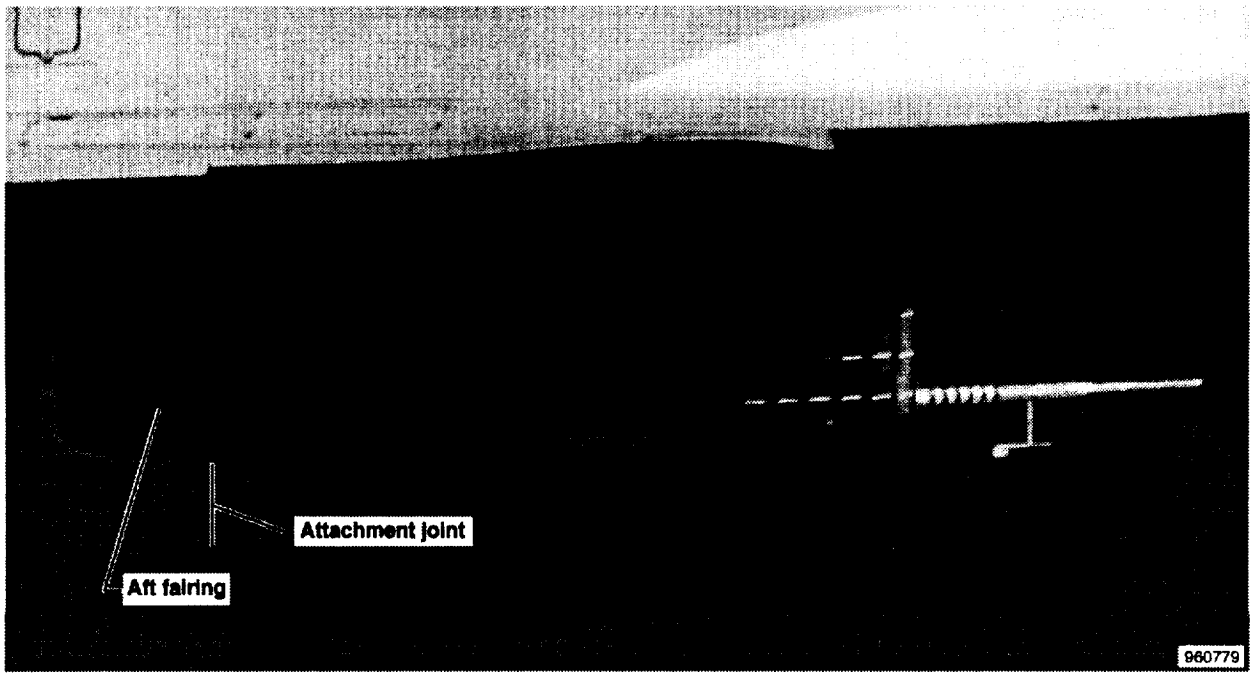

Figure 23. FTF-II with aft fairing and flow visualization results obtained in flight, right side with tufts; Mach = 0.70, $Hp \approx 45{,}000$ ft.

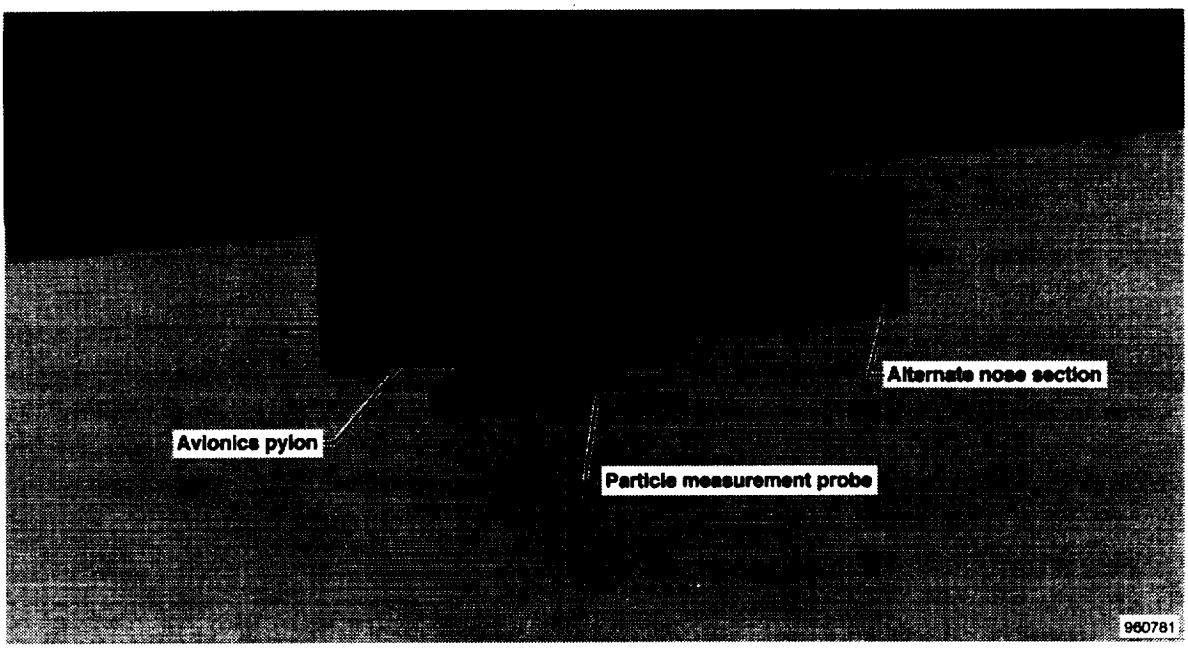

Figure 24. FTF–II configuration for the thermal protection systems durability program.

An important upgrade to the F-15B airplane was the installation of on-board video capability to document flight experiments. The current video coverage (aft left and front right video cameras) (fig. 25) should be sufficient for most flight experiments. Although the current video coverage is comprehensive, video camera locations can be modified to accommodate specific experiment requirements like the front left video camera (fig. 25).

Each configuration change will require an evaluation with respect to the fixture structure and experimental hardware. Typically, the best approach is to "over-design" experimental hardware so that flight safety issues can be resolved using simple and conservative engineering analyses. Configuration changes significantly different from the

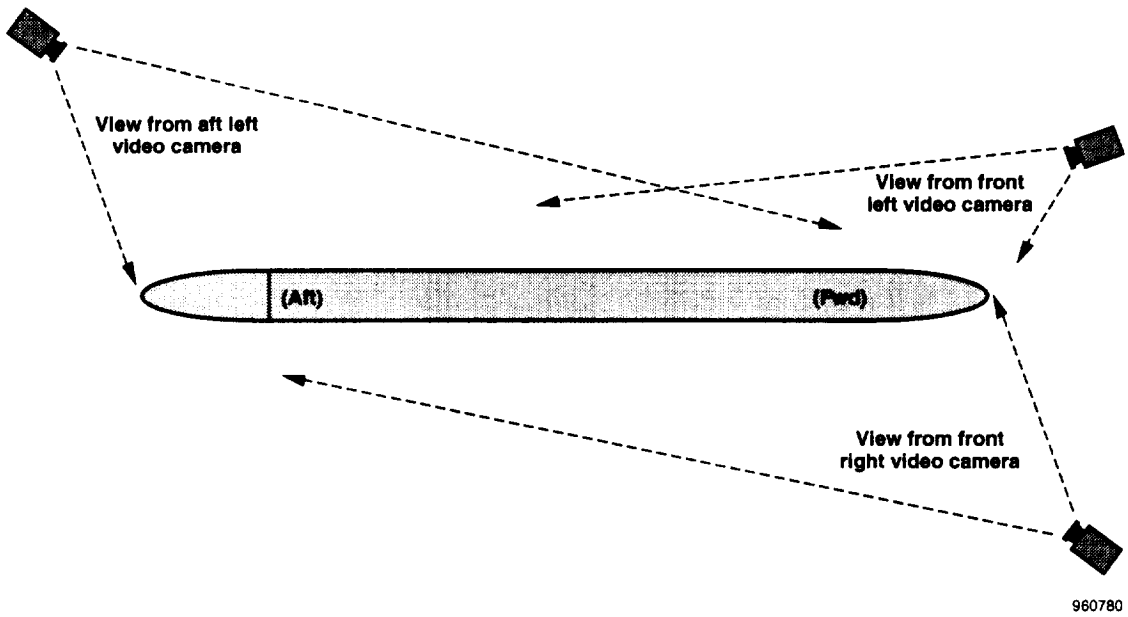

Figure 25. F-15B on-board video camera locations, top view.

current fin-like shape and area may require additional structural loads or aircraft stability analyses as appropriate. Appendices A and B contain further discussion of structural loads and aircraft stability considerations, respectively.

SUMMARY OF RESULTS

NASA Dryden Flight Research Center has developed the Flight Test Fixture II (FTF–II) for use as a generic test bed for aerodynamic and fluid mechanics research. The FTF–II is a low-aspect-ratio vertical fin-like shape that is mounted on the centerline of the F-15B lower fuselage and has flown at Mach numbers to a maximum of 2.0. The FTF–II is a composite structure with a modular configuration and removable components for functional flexibility.

Flow-quality data were primarily taken at 1-g flight conditions and a matrix of nominal altitudes of 15,000 ft, 30,000 ft, and 45,000 ft throughout the airspeed envelope of the aircraft. The flow environment was characterized using FTF–II noseboom airdata combined with surface pressure and boundary-layer measurements to survey aerodynamic flow quality. The FTF–II angle of attack at the trim aircraft angle of attack ranged from 1° at subsonic speeds to –9° at Mach 2.0. In general, chordwise pressure gradients were small aft of the nose section suction peak and recompression, except for the presence of a weak shock in the forward region of the FTF–II and base area effects. Boundary-layer thickness at the chordwise location $x/c = 0.90$ ranged from 1.25 in. to 1.45 in. with a slight increase in boundary-layer thickness at the supersonic Mach numbers.

Environmental conditions within the FTF–II were also documented to determine typical and extreme testing conditions. Projected worst-case internal temperatures within the FTF–II are –10 °F in flight to 145 °F during ground operations. The analysis of accelerometer data (x and z axis) indicates that $g_{rms} \leq 6.0$ for most flight conditions within the operational envelope of the F-15B/FTF–II.

Successful design of an FTF–II experiment by future investigators will require a basic understanding of established NASA Dryden policies and guidelines and alternate FTF–II configurations. The most relevant NASA Dryden documents for developing flight experiments on the FTF–II are the *Basic Operations Manual*, *Procedures for Objectives & Research Requirements Documents*, and *Process Specification Manual*. Alternate FTF–II configurations can be developed to satisfy a variety of flight test requirements, but these configurations must consider related operational and flight safety issues.

The FTF–II is a proven and documented flight test facility for aerodynamic and fluid mechanics research at speeds to a maximum Mach 2.0. Improvements to the F-15B performance, combined with a new FTF–II nose section and some additional analysis and verification of FTF–II loads and aircraft stability, could extend this limit as high as Mach 2.3.

ACKNOWLEDGMENTS

The author would like the thank the following contributors who provided valuable expertise and guidance toward this effort: Edwin J. Saltzman in the discipline of aerodynamics, Robert W. Kempel for issues related to aircraft stability, and Lawrence C. Freudinger in the reduction and analysis of acceleration data.

REFERENCES

[1] Meyer, Robert R., Jr., *A Unique Flight Test Facility: Description and Results*, NASA TM-84900, Nov. 1982.

[2] Montoya, Lawrence C., Brauns, David A., and Cissell, Ralph E., *Flight Experience With a Pivoting Traversing Boundary-Layer Probe*, NASA TM-X-56022, Jan. 1974.

[3] Chiles, Harry R. and Johnson, J. Blair, *Development of a Temperature-Compensated Hot-Film Anemometer System for Boundary-Layer Transition Detection on High-Performance Aircraft*, NASA TM-86732, Aug. 1985.

[4] Moes, Timothy R. and Meyer, Robert R., Jr., *In-Flight Investigation of Shuttle Tile Pressure Orifice Installations*, NASA TM-4219, Sept. 1990.

[5] Saltzman, Edwin J. and Hintz, John, *Flight Evaluation of Splitter-Plate Effectiveness in Reducing Base Drag at Mach Numbers From 0.65 to 0.90*, NASA TM-X-1376, May 1967.

[6] Trujillo, Bianca M. and Meyer, Robert R., Jr., *In-Flight Load Testing of Advanced Shuttle Thermal Protection Systems*, NASA TM-86024, Dec. 1983.

[7] Meyer, Robert. R., Jr. and Barneburg, Jack, *In-Flight Rain Damage Tests of the Shuttle Thermal Protection System*, NASA TM-100438, May 1988.

[8] Zuniga, Fanny A., Anderson, Bianca T., and Bertelrud, Arild, *Flight Test Results of Riblets at Supersonic Speeds*, NASA TM-4387, June 1992.

[9] Richwine, David M. and Del Frate, John H., *Development of a Low-Aspect Ratio Fin For Flight Research Experiments*, NASA TM-4596, Aug. 1994.

[10] Tanaka, Arthur Y. and Huete, Rodrigo J., "F/TF-15A Flying Qualities Air Force Development Test and Evaluation," AFFTC-TR-76-48, July 1977.

[11] United States Air Force, "Flight Manual: USAF Series F-15A/B/C/D Aircraft, Block 7 and Up," TO 1F-15A-1, July 1989.

[12] Schlichting, Hermann, *Boundary-Layer Theory,* McGraw-Hill, Inc. New York, 1979.

[13] Shapiro, Ascher H., *The Dynamics and Thermodynamics of Compressible Fluid Flow,* The Ronald Press Company, New York, 1953.

[14] Anderson, John D., Jr., *Hypersonic and High Temperature Gas Dynamics,* McGraw-Hill Book Company, New York, 1989.

APPENDIX A
STRUCTURAL LOAD CONSIDERATIONS FOR ALTERNATE CONFIGURATIONS

Major configuration changes to the Flight Test Fixture II (FTF–II) could have an impact on FTF–II loads and the F-15B airplane, depending on a variety of factors. The four load cells located at the sway braces (fig. 4(b)) can be used to validate side loads for rapid envelope expansion of major configuration changes. When needed, in-flight loads can be monitored and compared to prior loads documented in this report for the baseline fin-like configuration.

Flat-plate approximations were used to estimate FTF–II side loads in terms of aircraft limits, where side force, F_y, is approximated by $(\sin \beta)*q_\infty*A_s$.[9] Ground tests of the FTF–II mounted to the F-15B pylon (fig. A-1) were then conducted to correlate known applied side loads on the fixture to the measured resultant loads at the sway braces. By subtracting initial preloads (500–1000 lbf) at each sway pad and combining sway pad loads for each side, sway pad reaction loads, F_{sw}, were related directly to the applied moment, M_x, on the fixture. Figure A-2 shows this relationship was quite predictable and repeatable over several load cycles, where $F_{sw} = 39.4 + 0.385*M_x$.

Initial load assumptions, estimates, and factors of safety for the FTF–II design were quite conservative.[9] As a result, a design limit equivalent to $M_x = 48{,}368$ in-lbf (combined inertial and aerodynamic side loads[9]) was used for analysis of the fixture. Initial estimates were that an M_x equal to 48,368 in-lbf would result in an F_{sw} equal to 23,884 lbf. Determining actual loads using a linear extrapolation of ground test data indicates that the design limit $M_x = 48{,}368$ in-lbf would generate F_{sw} equal to 18,661 lbf. The difference between estimated and actual reaction loads is attributed to the indeterminate nature of the suspension lug/sway brace mounting structure. This result was also observed in the initial loads analysis and ground testing of a fixture test article.[9] The relevant aspect of this evaluation with respect to a flight experiment is that in-flight side loads that exceed the design limit of the FTF–II will indicate $F_{sw} \geq 18{,}661$ lbf.

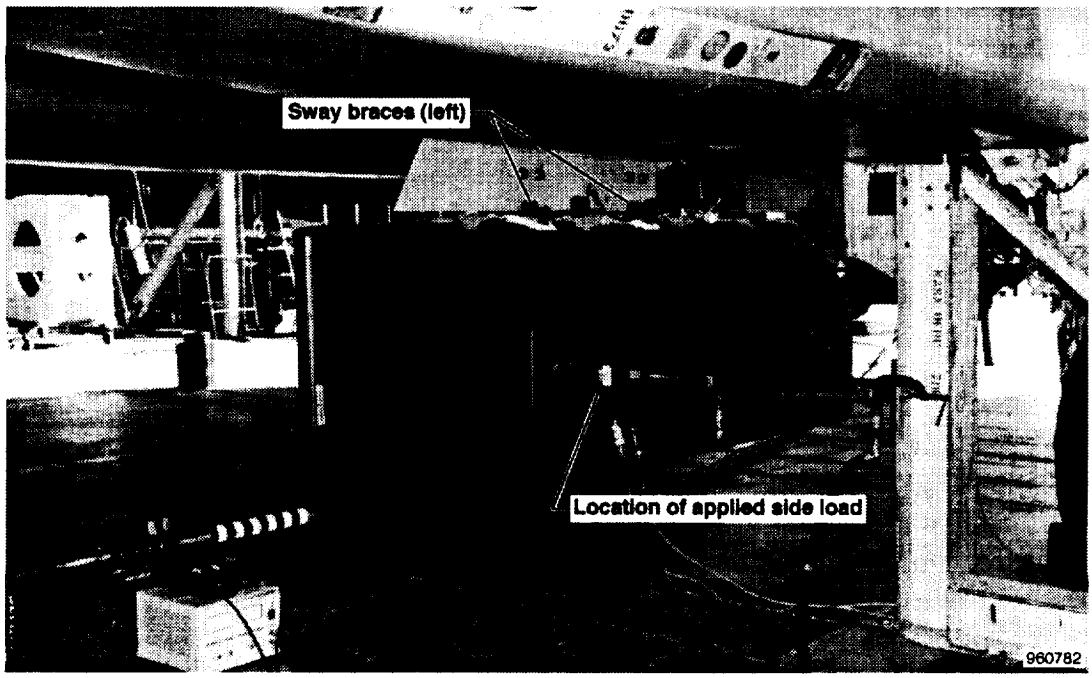

Figure A-1. Load testing of the FTF–II mounted to the F-15B pylon.

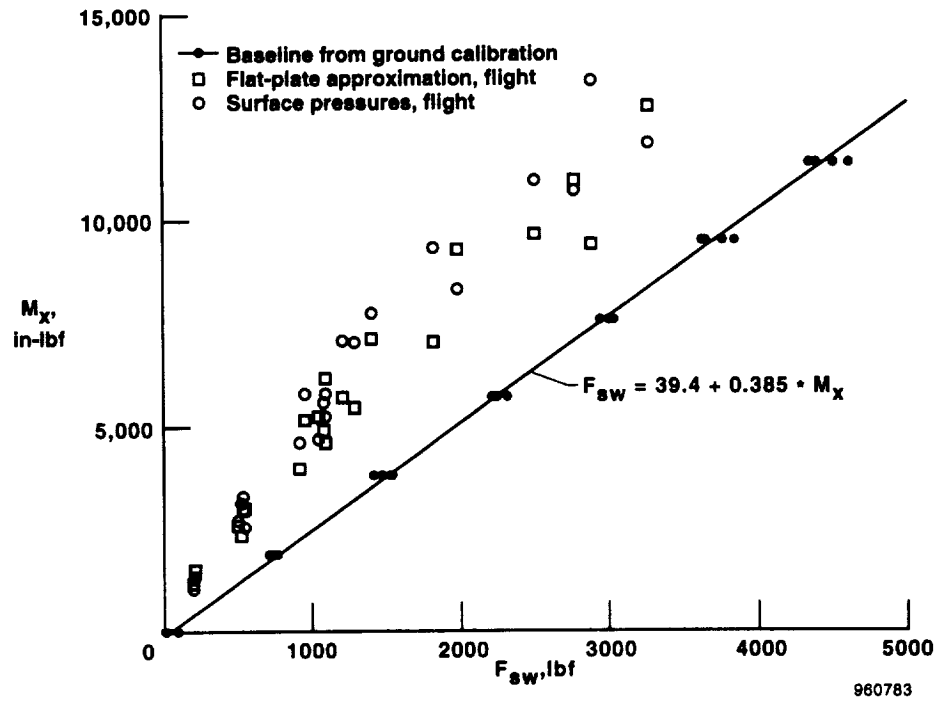

Figure A-2. The FTF–II reaction loads at the sway braces, flight- and ground-test data.

Further in-flight load evaluations were performed to gain additional confidence in estimated and actual loads. Integrated surface pressures and the flat-plate approximation using $z/b' = 0.50$ were calculated for the matrix of flight conditions. These techniques (fig. A-2) show reasonable agreement with each other but tend to overestimate flight loads by more than 50 percent for a given reaction load at the load cells. At the same time, flight data (fig. A-2) also reveal that existing F-15B control system limits, as observed from flight data, limit aircraft aerodynamic loads to less than 30 percent of FTF–II design limit side loads. These data imply that aerodynamic loads for any reasonable FTF–II configuration are fairly insignificant with respect to exceeding the design load. The primary area of future concern would be to avoid very dynamic maneuvers where high inertial loads in the lateral axis can be coupled with aerodynamic loads. As a simple and conservative rule, inspection of the FTF–II should be conducted if the total $F_{sw} \geq 10{,}000$ lbf (greater than 53.6 percent of FTF–II design limit side load) during flight test.

Major configuration changes to the FTF–II could also have an impact on the FTF–II center of pressure and the resulting distribution of loads on the fixture. Initial side force estimations for the baseline fin-like configuration[9] used a center of pressure of $x/c = 0.15$ to $x/c = 0.66$ for the estimation of aerodynamic loading. Further in-flight load evaluations at the matrix of flight conditions were performed using integrated surface pressures to document the actual FTF–II center of pressure.

The flight data (fig. A-3) indicate that the center of pressure estimations were valid, over a range in Mach numbers of 0.50 to 1.28, for an expected range of $x/c = 0.15$ to 0.66.[9] At subsonic speeds, the center of pressure ranges between $0.15 < x/c < 0.40$ with the farther aft locations at sideslip conditions where $\beta \geq 6°$. Limited sideslip data at Mach 1.28 show the general trend for the center of pressure to move slightly aft at supersonic speeds as well. Extrapolation of the flight results for the baseline fin-like configuration shows that development of a flight experiment requires only minimal consideration for the center of pressure location. In general, only major configuration changes or extensions of the nose section that would move the overall FTF–II center of pressure forward of the current $x/c = 0.15$ location would require further analysis.

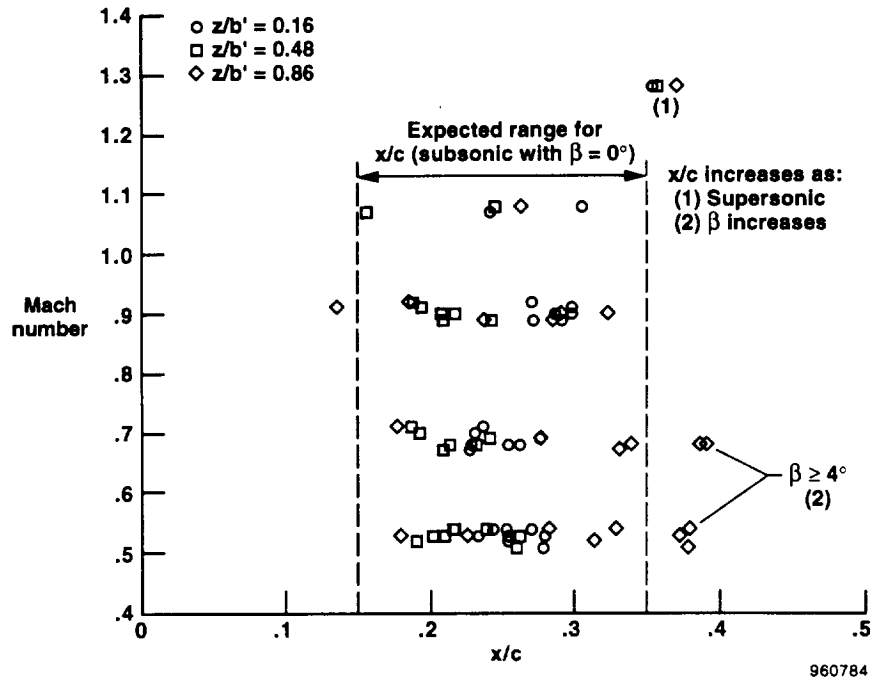

Figure A-3. Center of pressure locations determined from flight data as a function Mach number.

APPENDIX B
AIRCRAFT STABILITY CONSIDERATIONS FOR ALTERNATE CONFIGURATIONS

Major configuration changes to the FTF–II could have an impact on aircraft stability, depending on the size and location of the configuration change. Initial envelope expansion of the F-15B/FTF–II configuration (vertical fin) consisted of flight test of the FTF–II uninstrumented on the F-15B aircraft to perform envelope expansion[9] to a maximum of Mach 1.3 in the vertical fin configuration. Directional stability during phase one flight tests was evaluated by performing rudder doublets and making qualitative comparisons to the F-15B aircraft with and without a centerline tank. Comparisons at subsonic speeds indicated that the subsonic static directional stability, $C_{n\beta}$, derivative levels for the F-15B/FTF–II configuration were greater than 0.002/deg and had no adverse effects on aircraft stability.[9,10] Predictions also indicated that the $C_{n\beta}$ would decrease with increasing supersonic Mach numbers and approach levels as low as approximately 0.0005/deg at Mach ≥ 1.5. During phase two envelope expansion of the F-15B/FTF–II to Mach 1.8, several actions were taken by the project to understand and minimize the potential risk of reduced $C_{n\beta}$ caused by positioning the FTF–II at the centerline of the F-15B aircraft.

A study was performed to assess the risk of F-15 control augmentation system (CAS) disengagements and their impact on flight safety at reduced $C_{n\beta}$. The CAS disengagements were found to occur approximately once in every 200 flight hours and mostly during dynamic maneuvering. The CAS disengagements produced transients that were easily tolerated by the pilot and aircraft. In the case of a CAS failure, a 600-*KCAS* airspeed limit is imposed because of a mildly divergent longitudinal stability. In addition, a Mach 2.0 limit exists for the two-seat F-15 aircraft because pilots comments were that uncomfortable amounts of sideslip are produced. Overall, CAS disengagements at high speeds were found to result in handling qualities undesirable for sustained operations but quite acceptable for safe aircraft maneuvering.

An analysis of F-15 lateral–directional stability without the CAS, using a NASA Dryden batch simulation, was also performed for airspeeds to a maximum of Mach 2.2 at an altitude of 45,000 ft with particular attention to the dutch roll mode. Three linear models of an F-15 aircraft at a gross weight of 36,200 lbm were analyzed: one with predicted lateral–directional aerodynamics, one with aerodynamic increments caused by the FTF–II added, and one with reduced increments to match Air Force flight test data.[10] From these models, the damping ratio, ζ, and undamped natural frequency, ω_n, were calculated for the dutch roll mode and compared to MIL-F-8785C for Class IV aircraft (fighter) category B (cruise) handling qualities requirements. As figure B-1 shows, the addition of the FTF–II to the F-15B aircraft improved dutch roll damping at an altitude of 30,000 ft with sufficient stability at all flight conditions as predicted. Data at higher altitudes were also calculated and included with comparisons to flight test data.

F-15B/FTF–II envelope expansion was performed with rudder doublets to a maximum of Mach 1.8 with the CAS on and off for pilot evaluations and comparison to model predictions. Satisfactory-to-good damping was reported by the pilots with the CAS on or off at airspeeds to a maximum of Mach 1.8. Acceptable, but low-to-moderate, damping was noted at Mach ≥ 1.5. With the CAS off at Mach ≥ 1.5, pilot comments concurred with predictions of handling qualities undesirable for sustained operations but quite acceptable for safe aircraft recovery.

Flight data from the rudder doublets were also analyzed to calculate $\zeta*\omega_n$ for the dutch roll mode for comparison to predicted values (without the FTF–II, CAS off) and MIL-F-8785C (fig. B-2). Figure B-2 shows the flight data with the FTF–II installed and the CAS off. The F-15 airplane with the FTF–II installed appears to be more stable than predictions of an F-15 aircraft without FTF–II. As expected, $\zeta*\omega_n$ decreases with increasing altitude. At Mach 1.8 and an altitude of 45,000 ft, $\zeta*\omega_n$ is approximately 0.25 rad/sec, which is in the lower region of Level 3 handling qualities.

The final phase of F-15B/FTF–II envelope expansion was performed with rudder doublets to a maximum of Mach 2.0 with the CAS on. Maneuvers with the CAS off were not attempted at speeds greater than Mach 1.8. No large reductions in stability were observed, and pilot comments indicated that handling qualities were acceptable for safe aircraft maneuvering. Predicted trends indicate that the F-15/FTF–II dutch roll mode with the CAS on or off is stable at Mach ≤ 2.2. Additional evaluation of aircraft stability by performing rudder doublets with the CAS on is recommended for significant changes to the FTF–II or if envelope expansion of the current FTF–II configuration beyond Mach 2.0 at an altitude of 45,000 ft is desired.

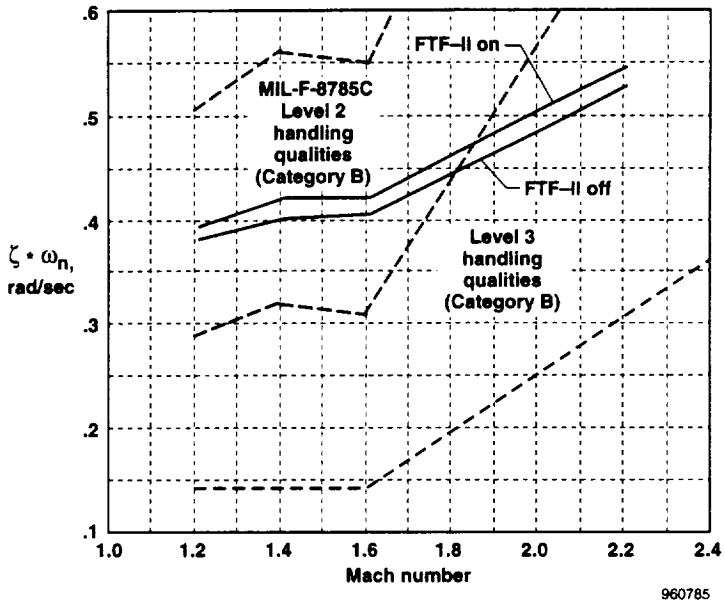

Figure B-1. The F-15B dutch roll mode damping obtained from NASA Dryden batch simulation (CAS off) with and without FTF–II; $Hp \approx 30{,}000$ feet, aircraft weight of 36,200 lbm.

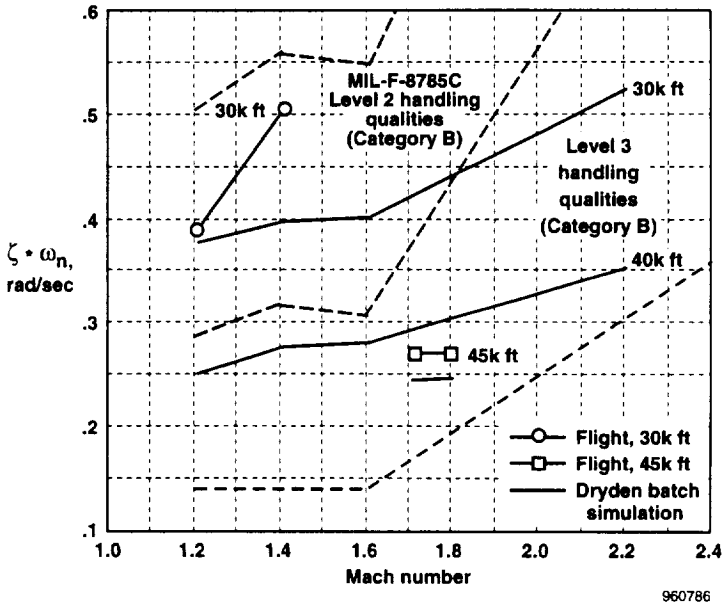

Figure B-2. Comparison of predicted and flight test values for F-15B dutch roll mode damping, CAS off, FTF–II on for flight, FTF–II on for simulation.

APPENDIX C
CHORDWISE PRESSURE DISTRIBUTION DATA

Table C-1. Steady-state chordwise pressure distribution data obtained in flight, $Hp \approx 15{,}000$ ft.

		Free-stream Mach number						
z/b	*x/c*	0.39	0.52	0.61	0.70	0.80	0.90	0.98
0.16	0.000	1.010	0.990	1.040	1.095	1.114	1.204	0.980
	0.025	-0.102	-0.112	-0.193	-0.248	-0.222	-0.108	0.000
	0.050	-0.183	-0.195	-0.285	-0.361	-0.370	-0.298	-0.169
	0.075	-0.197	-0.210	-0.305	-0.388	-0.413	-0.365	-0.241
	0.100	-0.216	-0.227	-0.320	-0.404	-0.437	-0.416	-0.290
	0.125	-0.202	-0.206	-0.299	-0.383	-0.413	-0.415	-0.297
	0.150	-0.154	-0.165	-0.253	-0.333	-0.360	-0.483	-0.354
	0.210	-0.086	-0.102	-0.184	-0.255	-0.274	-0.290	-0.203
	0.260	-0.113	-0.131	-0.217	-0.302	-0.353	-0.303	-0.335
	0.320	-0.088	-0.101	-0.179	-0.257	-0.306	-0.389	-0.357
	0.370	-0.072	-0.081	-0.155	-0.218	-0.244	-0.481	-0.410
	0.420	-0.055	-0.069	-0.137	-0.197	-0.214	-0.410	-0.381
	0.470	-0.065	-0.070	-0.139	-0.195	-0.212	-0.240	-0.422
	0.540	-0.053	-0.061	-0.126	-0.181	-0.195	-0.182	-0.346
	0.600	-0.036	-0.037	-0.102	-0.149	-0.151	-0.132	-0.220
	0.700	-0.019	-0.018	-0.075	-0.116	-0.117	-0.093	-0.115
	0.800	-0.035	-0.029	-0.084	-0.125	-0.126	-0.100	-0.111
	0.900	-0.048	-0.040	-0.091	-0.131	-0.127	-0.091	-0.069
	0.960	-0.180	-0.178	-0.228	-0.318	-0.377	-0.282	-0.212
0.48	0.000	1.019	1.007	1.040	1.096	1.111	1.203	0.930
	0.025	-0.119	-0.126	-0.209	-0.261	-0.225	-0.089	0.010
	0.050	-0.225	-0.234	-0.330	-0.417	-0.427	-0.327	-0.205
	0.075	-0.242	-0.259	-0.366	-0.471	-0.524	-0.460	-0.329
	0.100	-0.248	-0.264	-0.371	-0.477	-0.544	-0.576	-0.438
	0.125	-0.257	-0.265	-0.367	-0.464	-0.514	-0.656	-0.516
	0.150	-0.196	-0.205	-0.293	-0.377	-0.399	-0.654	-0.535
	0.210	-0.088	-0.096	-0.168	-0.228	-0.243	-0.123	-0.341
	0.260	-0.061	-0.069	-0.139	-0.202	-0.230	-0.173	-0.173
	0.320	-0.084	-0.079	-0.139	-0.198	-0.222	-0.277	-0.269
	0.370	-0.043	-0.047	-0.114	-0.173	-0.192	-0.352	-0.270
	0.420	-0.037	-0.041	-0.104	-0.156	-0.173	-0.361	-0.338
	0.470	-0.036	-0.037	-0.096	-0.150	-0.162	-0.144	-0.329
	0.540	-0.031	-0.033	-0.094	-0.141	-0.154	-0.143	-0.381
	0.600	-0.030	-0.026	-0.081	-0.127	-0.131	-0.115	-0.221
	0.700	-0.030	-0.022	-0.077	-0.117	-0.117	-0.099	-0.133
	0.800	-0.032	-0.027	-0.077	-0.117	-0.117	-0.094	-0.120
	0.900	-0.063	-0.058	-0.112	-0.152	-0.149	-0.106	-0.079
	0.960	-0.106	-0.101	-0.167	-0.223	-0.239	-0.189	-0.185
0.86	0.000	0.980	0.970	1.010	1.062	1.074	1.157	0.910
	0.025	-0.109	-0.131	-0.224	-0.300	-0.296	-0.182	-0.057
	0.050	-0.195	-0.213	-0.312	-0.409	-0.452	-0.425	-0.287
	0.075	-0.212	-0.227	-0.327	-0.426	-0.485	-0.482	-0.356
	0.100	-0.210	-0.229	-0.325	-0.423	-0.487	-0.560	-0.433
	0.125	-0.195	-0.197	-0.286	-0.375	-0.407	-0.611	-0.481
	0.150	-0.153	-0.169	-0.254	-0.328	-0.351	-0.647	-0.523
	0.210	-0.056	-0.065	-0.135	-0.190	-0.203	-0.084	-0.323
	0.260	-0.040	-0.043	-0.108	-0.160	-0.177	-0.143	-0.117
	0.320	-0.018	-0.028	-0.094	-0.147	-0.164	-0.206	-0.151
	0.370	-0.037	-0.037	-0.093	-0.145	-0.159	-0.242	-0.203
	0.420	-0.027	-0.023	-0.084	-0.132	-0.144	-0.271	-0.208
	0.470	-0.023	-0.019	-0.076	-0.124	-0.137	-0.146	-0.268
	0.540	-0.020	-0.020	-0.078	-0.126	-0.133	-0.128	-0.276
	0.600	-0.021	-0.016	-0.070	-0.113	-0.120	-0.111	-0.306
	0.700	-0.019	-0.016	-0.075	-0.117	-0.123	-0.110	-0.144
	0.800	-0.023	-0.016	-0.073	-0.113	-0.114	-0.096	-0.108
	0.900	-0.027	-0.027	-0.077	-0.107	-0.089	-0.010	0.020
	0.960	-0.148	-0.125	-0.185	-0.231	-0.228	-0.177	-0.151

Table C-2. Steady-state chordwise pressure distribution data obtained in flight, $Hp \approx 30{,}000$ ft.

		Free-stream Mach number										
z/b	*x/c*	0.51	0.62	0.70	0.79	0.89	1.00	1.05	1.15	1.28	1.39	1.48
0.16	0.000	1.005	1.045	1.092	1.132	1.207	1.202	1.246	1.330	1.307	1.149	1.045
	0.025	–0.075	–0.162	–0.190	–0.186	–0.091	0.020	0.090	0.200	0.280	0.250	0.280
	0.050	–0.172	–0.265	–0.315	–0.339	–0.277	–0.153	–0.098	–0.002	0.090	0.030	0.070
	0.075	–0.183	–0.282	–0.342	–0.378	–0.335	–0.211	–0.156	–0.090	0.000	–0.072	–0.040
	0.100	–0.196	–0.301	–0.357	–0.398	–0.394	–0.263	–0.206	–0.158	–0.071	–0.167	–0.123
	0.125	–0.181	–0.279	–0.343	–0.379	–0.391	–0.269	–0.204	–0.147	–0.061	–0.218	–0.187
	0.150	–0.136	–0.232	–0.289	–0.323	–0.448	–0.316	–0.243	–0.163	–0.065	–0.138	–0.229
	0.210	–0.070	–0.161	–0.215	–0.243	–0.172	–0.168	–0.097	–0.010	0.090	0.090	0.050
	0.260	–0.105	–0.200	–0.264	–0.313	–0.280	–0.311	–0.258	–0.204	–0.100	–0.051	–0.042
	0.320	–0.075	–0.166	–0.225	–0.262	–0.369	–0.360	–0.315	–0.309	–0.213	–0.153	–0.113
	0.370	–0.057	–0.133	–0.183	–0.211	–0.289	–0.387	–0.312	–0.291	–0.199	–0.167	–0.127
	0.420	–0.047	–0.123	–0.169	–0.186	–0.154	–0.350	–0.308	–0.265	–0.234	–0.227	–0.182
	0.470	–0.050	–0.124	–0.169	–0.184	–0.156	–0.369	–0.313	–0.255	–0.213	–0.194	–0.200
	0.540	–0.046	–0.116	–0.159	–0.172	–0.145	–0.313	–0.357	–0.354	–0.268	–0.237	–0.213
	0.600	–0.020	–0.085	–0.122	–0.132	–0.093	–0.164	–0.215	–0.358	–0.287	–0.260	–0.229
	0.700	–0.002	–0.067	–0.096	–0.098	–0.054	–0.070	–0.040	–0.127	–0.283	–0.324	–0.297
	0.800	–0.024	–0.079	–0.108	–0.108	–0.063	–0.074	–0.034	–0.006	–0.078	–0.213	–0.204
	0.900	–0.031	–0.083	–0.116	–0.109	–0.058	–0.035	0.010	0.030	0.010	–0.101	–0.243
	0.960	–0.138	–0.221	–0.287	–0.339	–0.275	–0.171	–0.090	0.010	0.090	0.040	–0.006
0.48	0.000	1.011	1.048	1.094	1.131	1.203	1.198	1.251	1.327	1.252	1.102	1.004
	0.025	–0.096	–0.178	–0.203	–0.189	–0.073	0.040	0.120	0.220	0.320	0.330	0.360
	0.050	–0.206	–0.308	–0.367	–0.398	–0.315	–0.177	–0.104	0.000	0.100	0.110	0.150
	0.075	–0.231	–0.339	–0.418	–0.479	–0.436	–0.295	–0.223	–0.120	–0.024	–0.025	0.010
	0.100	–0.231	–0.347	–0.427	–0.501	–0.541	–0.398	–0.322	–0.229	–0.127	–0.132	–0.092
	0.125	–0.237	–0.346	–0.420	–0.475	–0.614	–0.478	–0.405	–0.326	–0.215	–0.225	–0.184
	0.150	–0.181	–0.274	–0.338	–0.374	–0.602	–0.496	–0.423	–0.374	–0.262	–0.274	–0.238
	0.210	–0.079	–0.149	–0.199	–0.216	–0.122	–0.319	–0.270	–0.256	–0.185	–0.308	–0.283
	0.260	–0.046	–0.126	–0.171	–0.199	–0.183	–0.132	–0.069	–0.105	–0.060	–0.077	–0.212
	0.320	–0.070	–0.139	–0.179	–0.201	–0.252	–0.244	–0.154	–0.095	–0.056	–0.064	–0.079
	0.370	–0.031	–0.103	–0.144	–0.163	–0.198	–0.232	–0.183	–0.155	–0.085	–0.056	–0.048
	0.420	–0.021	–0.090	–0.129	–0.144	–0.122	–0.300	–0.225	–0.157	–0.074	–0.076	–0.043
	0.470	–0.011	–0.086	–0.127	–0.139	–0.112	–0.273	–0.217	–0.202	–0.128	–0.102	–0.082
	0.540	–0.017	–0.081	–0.118	–0.129	–0.101	–0.336	–0.280	–0.195	–0.158	–0.140	–0.108
	0.600	–0.016	–0.073	–0.107	–0.112	–0.077	–0.141	–0.318	–0.246	–0.185	–0.163	–0.140
	0.700	–0.005	–0.069	–0.097	–0.100	–0.058	–0.080	–0.054	–0.307	–0.218	–0.197	–0.205
	0.800	–0.012	–0.069	–0.099	–0.098	–0.055	–0.074	–0.023	–0.013	–0.235	–0.235	–0.228
	0.900	–0.050	–0.105	–0.130	–0.127	–0.078	–0.036	0.030	0.070	0.000	–0.158	–0.214
	0.960	–0.087	–0.160	–0.202	–0.216	–0.170	–0.134	–0.061	0.050	0.090	–0.085	–0.143
0.86	0.000	0.970	1.012	1.059	1.093	1.167	1.173	1.178	1.270	1.224	1.079	0.980
	0.025	–0.090	–0.187	–0.239	–0.253	–0.159	–0.025	0.030	0.150	0.250	0.270	0.300
	0.050	–0.186	–0.288	–0.359	–0.409	–0.388	–0.253	–0.175	–0.068	0.020	0.040	0.080
	0.075	–0.207	–0.308	–0.384	–0.446	–0.451	–0.320	–0.242	–0.170	–0.084	–0.057	–0.017
	0.100	–0.201	–0.308	–0.382	–0.449	–0.525	–0.393	–0.317	–0.246	–0.166	–0.168	–0.125
	0.125	–0.186	–0.270	–0.339	–0.384	–0.558	–0.439	–0.365	–0.299	–0.218	–0.223	–0.182
	0.150	–0.151	–0.242	–0.300	–0.331	–0.569	–0.482	–0.408	–0.350	–0.266	–0.271	–0.238
	0.210	–0.043	–0.120	–0.163	–0.177	–0.119	–0.290	–0.249	–0.256	–0.180	–0.199	–0.208
	0.260	–0.030	–0.102	–0.141	–0.156	–0.138	–0.082	–0.017	–0.165	–0.152	–0.191	–0.190
	0.320	–0.007	–0.078	–0.122	–0.139	–0.149	–0.128	–0.072	–0.021	0.010	–0.126	–0.205
	0.370	–0.026	–0.091	–0.125	–0.139	–0.138	–0.175	–0.113	–0.075	–0.008	0.010	–0.040
	0.420	–0.013	–0.075	–0.110	–0.123	–0.106	–0.173	–0.117	–0.101	–0.034	–0.013	0.010
	0.470	–0.005	–0.069	–0.104	–0.115	–0.091	–0.231	–0.162	–0.087	–0.067	–0.065	–0.030
	0.540	–0.010	–0.071	–0.105	–0.113	–0.085	–0.235	–0.189	–0.152	–0.087	–0.077	–0.073
	0.600	–0.006	–0.065	–0.098	–0.101	–0.067	–0.260	–0.202	–0.139	–0.104	–0.100	–0.078
	0.700	0.000	–0.062	–0.094	–0.099	–0.063	–0.088	–0.088	–0.207	–0.143	–0.134	–0.112
	0.800	–0.011	–0.063	–0.097	–0.094	–0.055	–0.066	–0.022	–0.171	–0.175	–0.156	–0.133
	0.900	–0.016	–0.072	–0.094	–0.078	–0.001	0.060	0.120	0.160	0.040	–0.026	–0.023
	0.960	–0.120	–0.182	–0.215	–0.212	–0.150	–0.112	–0.055	–0.012	–0.082	–0.241	–0.248

Table C-3. Steady-state chordwise pressure distribution data obtained in flight, $Hp \approx 45{,}000$ ft.

		Free-stream Mach number													
z/b	*x/c*	0.70	0.79	0.90	0.98	1.06	1.16	1.28	1.39	1.49	1.60	1.69	1.80	1.90	2.00
0.16	0.000	1.110	1.147	1.220	1.220	1.232	1.339	1.447	1.450	1.431	1.370	1.461	1.499	1.424	1.317
	0.025	–0.202	–0.190	–0.103	–0.006	0.060	0.190	0.260	0.260	0.270	0.290	0.360	0.390	0.420	0.420
	0.050	–0.334	–0.351	–0.300	–0.202	–0.138	–0.017	0.060	0.040	0.070	0.110	0.170	0.220	0.250	0.270
	0.075	–0.360	–0.397	–0.366	–0.261	–0.215	–0.107	–0.019	–0.058	–0.029	0.000	0.060	0.110	0.140	0.180
	0.100	–0.368	–0.409	–0.414	–0.304	–0.268	–0.176	–0.080	–0.157	–0.119	–0.076	–0.023	0.020	0.060	0.090
	0.125	–0.346	–0.387	–0.413	–0.309	–0.258	–0.165	–0.068	–0.215	–0.182	–0.141	–0.089	–0.038	–0.005	0.020
	0.150	–0.294	–0.328	–0.465	–0.347	–0.282	–0.177	–0.070	–0.171	–0.224	–0.192	–0.143	–0.093	–0.057	–0.024
	0.210	–0.206	–0.238	–0.201	–0.182	–0.121	–0.012	0.090	0.100	0.040	–0.003	0.010	0.030	0.030	0.020
	0.260	–0.261	–0.322	–0.282	–0.349	–0.321	–0.223	–0.104	–0.045	–0.042	–0.043	0.000	0.040	0.070	0.080
	0.320	–0.220	–0.263	–0.382	–0.375	–0.414	–0.340	–0.222	–0.157	–0.117	–0.113	–0.056	–0.004	0.030	0.050
	0.370	–0.180	–0.213	–0.479	–0.422	–0.381	–0.311	–0.206	–0.168	–0.133	–0.121	–0.074	–0.020	0.010	0.040
	0.420	–0.164	–0.188	–0.181	–0.370	–0.361	–0.288	–0.240	–0.219	–0.174	–0.143	–0.097	–0.053	–0.018	0.010
	0.470	–0.162	–0.188	–0.166	–0.382	–0.353	–0.292	–0.206	–0.188	–0.193	–0.176	–0.127	–0.092	–0.058	–0.024
	0.540	–0.161	–0.173	–0.165	–0.242	–0.438	–0.390	–0.286	–0.243	–0.215	–0.219	–0.186	–0.152	–0.117	–0.080
	0.600	–0.125	–0.132	–0.110	–0.119	–0.290	–0.401	–0.315	–0.267	–0.234	–0.225	–0.194	–0.163	–0.141	–0.111
	0.700	–0.100	–0.100	–0.076	–0.054	–0.110	–0.167	–0.311	–0.325	–0.290	–0.258	–0.224	–0.192	–0.171	–0.165
	0.800	–0.111	–0.110	–0.086	–0.050	–0.059	–0.052	–0.088	–0.222	–0.205	–0.233	–0.195	–0.161	–0.147	–0.146
	0.900	–0.125	–0.122	–0.081	–0.025	–0.024	0.000	0.000	–0.087	–0.236	–0.244	–0.209	–0.166	–0.142	–0.123
	0.960	–0.314	–0.363	–0.286	–0.193	–0.124	–0.001	0.090	0.050	–0.016	–0.144	–0.110	–0.075	–0.062	–0.053
0.48	0.000	1.120	1.153	1.225	1.226	1.251	1.335	1.426	1.431	1.424	1.505	1.503	1.443	1.372	1.270
	0.025	–0.220	–0.189	–0.079	0.020	0.090	0.210	0.310	0.340	0.360	0.380	0.450	0.510	0.510	0.530
	0.050	–0.387	–0.405	–0.326	–0.210	–0.134	–0.006	0.080	0.120	0.140	0.170	0.230	0.280	0.320	0.320
	0.075	–0.428	–0.491	–0.452	–0.331	–0.260	–0.130	–0.034	–0.013	0.010	0.050	0.100	0.160	0.190	0.210
	0.100	–0.431	–0.513	–0.561	–0.436	–0.368	–0.237	–0.135	–0.119	–0.085	–0.052	0.000	0.050	0.090	0.120
	0.125	–0.436	–0.493	–0.643	–0.523	–0.462	–0.340	–0.231	–0.217	–0.180	–0.134	–0.082	–0.027	0.000	0.030
	0.150	–0.345	–0.377	–0.636	–0.528	–0.493	–0.380	–0.273	–0.273	–0.234	–0.193	–0.143	–0.094	–0.055	–0.026
	0.210	–0.195	–0.218	–0.100	–0.339	–0.340	–0.280	–0.196	–0.322	–0.277	–0.231	–0.180	–0.132	–0.101	–0.068
	0.260	–0.174	–0.202	–0.164	–0.134	–0.141	–0.126	–0.065	–0.081	–0.229	–0.256	–0.206	–0.148	–0.122	–0.089
	0.320	–0.203	–0.219	–0.293	–0.260	–0.197	–0.135	–0.074	–0.063	–0.086	–0.148	–0.111	–0.074	–0.059	–0.079
	0.370	–0.153	–0.170	–0.320	–0.240	–0.266	–0.183	–0.095	–0.052	–0.045	–0.132	–0.100	–0.071	–0.050	–0.029
	0.420	–0.132	–0.149	–0.143	–0.307	–0.267	–0.180	–0.082	–0.053	–0.024	–0.103	–0.074	–0.056	–0.043	–0.027
	0.470	–0.130	–0.143	–0.121	–0.270	–0.278	–0.235	–0.136	–0.102	–0.079	–0.082	–0.064	–0.037	–0.022	–0.015
	0.540	–0.122	–0.137	–0.119	–0.295	–0.303	–0.246	–0.172	–0.133	–0.101	–0.097	–0.063	–0.057	–0.036	–0.018
	0.600	–0.116	–0.117	–0.093	–0.106	–0.364	–0.277	–0.195	–0.169	–0.143	–0.125	–0.090	–0.062	–0.056	–0.034
	0.700	–0.111	–0.105	–0.080	–0.049	–0.114	–0.322	–0.242	–0.196	–0.196	–0.177	–0.134	–0.105	–0.087	–0.083
	0.800	–0.109	–0.102	–0.073	–0.035	–0.046	–0.064	–0.260	–0.241	–0.230	–0.220	–0.176	–0.136	–0.110	–0.106
	0.900	–0.152	–0.145	–0.096	–0.024	0.000	0.040	–0.008	–0.168	–0.199	–0.231	–0.196	–0.145	–0.127	–0.110
	0.960	–0.225	–0.232	–0.171	–0.114	–0.066	0.030	0.080	–0.066	–0.144	–0.178	–0.157	–0.124	–0.104	–0.090
0.86	0.000	1.091	1.121	1.196	1.198	1.187	1.313	1.433	1.435	1.398	1.400	1.472	1.414	1.347	1.247
	0.025	–0.218	–0.229	–0.148	–0.044	0.030	0.150	0.260	0.290	0.300	0.300	0.370	0.370	0.400	0.420
	0.050	–0.348	–0.399	–0.383	–0.278	–0.194	–0.074	0.020	0.060	0.090	0.120	0.180	0.230	0.260	0.290
	0.075	–0.374	–0.442	–0.447	–0.340	–0.278	–0.174	–0.091	–0.052	–0.017	0.010	0.070	0.120	0.150	0.180
	0.100	–0.374	–0.439	–0.526	–0.414	–0.355	–0.254	–0.173	–0.151	–0.115	–0.078	–0.023	0.020	0.060	0.090
	0.125	–0.345	–0.403	–0.573	–0.459	–0.409	–0.305	–0.218	–0.210	–0.177	–0.146	–0.094	–0.043	–0.013	0.010
	0.150	–0.289	–0.324	–0.597	–0.497	–0.452	–0.351	–0.266	–0.259	–0.230	–0.199	–0.149	–0.098	–0.067	–0.042
	0.210	–0.153	–0.173	–0.063	–0.331	–0.336	–0.260	–0.187	–0.211	–0.205	–0.204	–0.161	–0.113	–0.087	–0.070
	0.260	–0.139	–0.156	–0.132	–0.087	–0.148	–0.221	–0.157	–0.173	–0.174	–0.165	–0.131	–0.094	–0.072	–0.051
	0.320	–0.113	–0.136	–0.181	–0.137	–0.126	–0.031	0.000	–0.131	–0.197	–0.171	–0.130	–0.094	–0.072	–0.046
	0.370	–0.129	–0.142	–0.203	–0.182	–0.151	–0.107	–0.014	0.010	–0.055	–0.184	–0.139	–0.098	–0.078	–0.060
	0.420	–0.106	–0.125	–0.136	–0.170	–0.183	–0.120	–0.041	–0.010	0.010	–0.111	–0.119	–0.100	–0.080	–0.056
	0.470	–0.102	–0.116	–0.109	–0.231	–0.181	–0.150	–0.072	–0.061	–0.023	–0.076	–0.048	–0.022	–0.019	–0.041
	0.540	–0.102	–0.114	–0.103	–0.215	–0.219	–0.196	–0.089	–0.075	–0.076	–0.054	–0.038	–0.020	–0.001	0.010
	0.600	–0.097	–0.105	–0.088	–0.150	–0.237	–0.166	–0.121	–0.091	–0.073	–0.081	–0.044	–0.035	–0.016	0.000
	0.700	–0.083	–0.093	–0.075	–0.042	–0.322	–0.218	–0.157	–0.123	–0.106	–0.110	–0.077	–0.048	–0.042	–0.027
	0.800	–0.095	–0.097	–0.072	–0.032	–0.067	–0.251	–0.173	–0.154	–0.135	–0.139	–0.100	–0.060	–0.050	–0.047
	0.900	–0.085	–0.072	0.000	0.080	0.100	0.130	0.010	–0.041	–0.033	–0.149	–0.058	0.000	0.010	0.030
	0.960	–0.228	–0.224	–0.165	–0.101	–0.070	–0.040	–0.105	–0.246	–0.244	–0.330	–0.282	–0.181	–0.180	–0.183
	$C_{p_{max}}$	1.12	1.17	1.22	1.26	1.31	1.37	1.43	1.48	1.52	1.56	1.59	1.62	1.64	1.66

Table C-4. Chordwise pressure distribution data, obtained in flight, as a function of angle of sideslip, Mach = 0.52 and 0.70.

		M = 0.52, $Hp \approx$ 15,000 ft					M = 0.70, $Hp \approx$ 45,000 ft				
	β	8.04	3.95	0.00	−3.98	−8.00	8.02	4.01	−0.06	−3.98	−7.99
z/b	*x/c*										
0.16	0.000	0.800	0.950	1.007	0.940	0.790	0.920	1.046	1.089	1.058	0.910
	0.025	−0.564	−0.359	−0.136	0.060	0.260	−0.749	−0.487	−0.212	0.000	0.230
	0.050	−0.495	−0.363	−0.213	−0.070	0.080	−0.667	−0.503	−0.323	−0.168	0.010
	0.075	−0.446	−0.339	−0.226	−0.111	0.020	−0.598	−0.487	−0.342	−0.225	−0.058
	0.100	−0.433	−0.341	−0.237	−0.138	−0.022	−0.591	−0.472	−0.350	−0.248	−0.092
	0.125	−0.403	−0.310	−0.218	−0.132	−0.022	−0.566	−0.446	−0.323	−0.227	−0.086
	0.150	−0.341	−0.260	−0.173	−0.094	0.000	−0.496	−0.382	−0.276	−0.186	−0.053
	0.210	−0.231	−0.173	−0.104	−0.043	0.040	−0.347	−0.259	−0.190	−0.124	0.000
	0.260	−0.233	−0.186	−0.133	−0.085	−0.010	−0.367	−0.304	−0.231	−0.179	−0.081
	0.320	−0.181	−0.143	−0.105	−0.065	0.000	−0.291	−0.237	−0.197	−0.154	−0.061
	0.370	−0.137	−0.116	−0.083	−0.050	0.000	−0.230	−0.201	−0.166	−0.128	−0.053
	0.420	−0.108	−0.090	−0.067	−0.043	0.010	−0.196	−0.170	−0.146	−0.119	−0.053
	0.470	−0.101	−0.089	−0.075	−0.045	0.000	−0.183	−0.180	−0.152	−0.125	−0.072
	0.540	−0.089	−0.080	−0.059	−0.036	0.000	−0.175	−0.161	−0.155	−0.126	−0.064
	0.600	−0.057	−0.056	−0.037	−0.016	0.020	−0.141	−0.121	−0.114	−0.088	−0.045
	0.700	−0.032	−0.026	−0.018	−0.003	0.030	−0.106	−0.096	−0.096	−0.074	−0.034
	0.800	−0.031	−0.030	−0.027	−0.019	0.000	−0.118	−0.112	−0.105	−0.099	−0.064
	0.900	−0.042	−0.037	−0.038	−0.033	−0.015	−0.118	−0.121	−0.120	−0.115	−0.080
	0.960	−0.193	−0.189	−0.174	−0.186	−0.176	−0.318	−0.304	−0.288	−0.286	−0.273
0.48	0.000	0.780	0.950	1.007	0.940	0.750	0.930	1.061	1.096	1.053	0.880
	0.025	−0.628	−0.395	−0.152	0.060	0.270	−0.852	−0.529	−0.227	0.000	0.250
	0.050	−0.542	−0.409	−0.250	−0.095	0.070	−0.775	−0.575	−0.374	−0.198	0.000
	0.075	−0.490	−0.390	−0.272	−0.154	−0.019	−0.677	−0.550	−0.408	−0.277	−0.098
	0.100	−0.434	−0.361	−0.276	−0.182	−0.061	−0.606	−0.509	−0.405	−0.306	−0.160
	0.125	−0.395	−0.347	−0.273	−0.198	−0.095	−0.564	−0.491	−0.412	−0.333	−0.189
	0.150	−0.307	−0.262	−0.210	−0.148	−0.063	−0.442	−0.384	−0.325	−0.264	−0.155
	0.210	−0.160	−0.137	−0.098	−0.057	0.000	−0.261	−0.235	−0.193	−0.137	−0.058
	0.260	−0.117	−0.095	−0.066	−0.036	0.010	−0.218	−0.190	−0.162	−0.119	−0.042
	0.320	−0.115	−0.100	−0.078	−0.046	−0.001	−0.235	−0.220	−0.190	−0.163	−0.088
	0.370	−0.076	−0.067	−0.047	−0.023	0.020	−0.169	−0.159	−0.134	−0.105	−0.053
	0.420	−0.061	−0.054	−0.042	−0.015	0.010	−0.146	−0.140	−0.120	−0.097	−0.050
	0.470	−0.055	−0.046	−0.037	−0.017	0.020	−0.138	−0.124	−0.118	−0.100	−0.034
	0.540	−0.042	−0.039	−0.030	−0.017	0.010	−0.130	−0.129	−0.117	−0.090	−0.053
	0.600	−0.028	−0.033	−0.021	−0.010	0.020	−0.123	−0.105	−0.110	−0.088	−0.045
	0.700	−0.021	−0.027	−0.019	−0.010	0.010	−0.113	−0.118	−0.100	−0.083	−0.054
	0.800	−0.023	−0.027	−0.021	−0.013	0.010	−0.100	−0.105	−0.093	−0.091	−0.055
	0.900	−0.044	−0.052	−0.050	−0.045	−0.027	−0.135	−0.132	−0.140	−0.125	−0.107
	0.960	−0.094	−0.101	−0.097	−0.098	−0.093	−0.198	−0.209	−0.207	−0.207	−0.200
0.86	0.000	0.830	0.950	0.970	0.900	0.710	0.930	1.063	1.074	1.009	0.810
	0.025	−0.502	−0.328	−0.154	0.010	0.190	−0.680	−0.442	−0.208	−0.023	0.200
	0.050	−0.416	−0.337	−0.227	−0.117	0.000	−0.606	−0.474	−0.333	−0.208	−0.055
	0.075	−0.362	−0.315	−0.232	−0.164	−0.062	−0.512	−0.446	−0.350	−0.261	−0.143
	0.100	−0.332	−0.295	−0.234	−0.179	−0.093	−0.487	−0.425	−0.354	−0.292	−0.185
	0.125	−0.273	−0.247	−0.199	−0.171	−0.104	−0.413	−0.364	−0.316	−0.273	−0.186
	0.150	−0.224	−0.207	−0.171	−0.143	−0.084	−0.352	−0.319	−0.270	−0.244	−0.166
	0.210	−0.116	−0.084	−0.066	−0.044	−0.008	−0.222	−0.168	−0.133	−0.117	−0.051
	0.260	−0.080	−0.060	−0.043	−0.027	0.000	−0.188	−0.153	−0.127	−0.105	−0.057
	0.320	−0.061	−0.045	−0.027	−0.013	0.010	−0.159	−0.127	−0.102	−0.085	−0.040
	0.370	−0.067	−0.052	−0.033	−0.021	0.000	−0.183	−0.146	−0.126	−0.102	−0.070
	0.420	−0.049	−0.032	−0.027	−0.012	0.010	−0.161	−0.124	−0.100	−0.088	−0.047
	0.470	−0.043	−0.033	−0.014	−0.012	0.010	−0.158	−0.117	−0.096	−0.072	−0.056
	0.540	−0.052	−0.032	−0.022	−0.011	0.000	−0.178	−0.114	−0.096	−0.084	−0.054
	0.600	−0.051	−0.024	−0.013	−0.005	0.010	−0.183	−0.112	−0.089	−0.077	−0.052
	0.700	−0.066	−0.029	−0.013	−0.011	0.000	−0.197	−0.107	−0.073	−0.067	−0.040
	0.800	−0.073	−0.029	−0.012	−0.010	0.000	−0.201	−0.121	−0.091	−0.084	−0.062
	0.900	−0.138	−0.039	−0.023	−0.053	−0.062	−0.286	−0.154	−0.083	−0.099	−0.119
	0.960	−0.159	−0.142	−0.119	−0.124	−0.107	−0.284	−0.264	−0.224	−0.219	−0.192

Table C–5. Chordwise pressure distribution data, obtained in flight, as a function of angle of sideslip, Mach = 0.89 and 1.28.

		M = 0.89, $Hp \approx 45{,}000$ ft					M = 1.28, $Hp \approx 45{,}000$ ft				
	β	7.96	3.99	–0.03	–3.82	–7.97	3.57	1.93	–0.07	–2.02	–3.59
z/b'	*x/c*										
0.16	0.000	1.112	1.189	1.216	1.188	1.104	1.407	1.445	1.411	1.360	1.381
	0.025	–0.537	–0.358	–0.111	0.090	0.300	0.090	0.200	0.360	0.420	0.510
	0.050	–0.669	–0.524	–0.306	–0.140	0.050	–0.104	0.000	0.150	0.190	0.280
	0.075	–0.641	–0.524	–0.375	–0.237	–0.061	–0.192	–0.077	0.040	0.070	0.130
	0.100	–0.641	–0.545	–0.415	–0.293	–0.124	–0.224	–0.114	–0.056	–0.025	0.020
	0.125	–0.639	–0.552	–0.423	–0.281	–0.129	–0.183	–0.098	–0.117	–0.027	0.040
	0.150	–0.712	–0.596	–0.472	–0.320	–0.104	–0.149	–0.083	–0.160	–0.002	0.050
	0.210	–0.606	–0.422	–0.186	–0.137	–0.046	–0.054	0.060	0.180	0.120	0.180
	0.260	–0.684	–0.393	–0.288	–0.260	–0.191	–0.176	–0.105	0.020	–0.055	–0.001
	0.320	–0.565	–0.324	–0.378	–0.323	–0.265	–0.294	–0.230	–0.063	–0.178	–0.127
	0.370	–0.430	–0.503	–0.471	–0.286	–0.118	–0.277	–0.231	–0.083	–0.174	–0.122
	0.420	–0.214	–0.195	–0.170	–0.138	–0.102	–0.250	–0.241	–0.137	–0.218	–0.175
	0.470	–0.225	–0.197	–0.164	–0.147	–0.120	–0.242	–0.210	–0.139	–0.194	–0.139
	0.540	–0.209	–0.180	–0.164	–0.144	–0.109	–0.324	–0.280	–0.170	–0.268	–0.224
	0.600	–0.164	–0.130	–0.114	–0.094	–0.059	–0.353	–0.319	–0.194	–0.285	–0.239
	0.700	–0.133	–0.091	–0.076	–0.057	–0.028	–0.322	–0.326	–0.253	–0.260	–0.204
	0.800	–0.127	–0.098	–0.082	–0.075	–0.045	–0.122	–0.097	–0.160	–0.094	–0.062
	0.900	–0.111	–0.100	–0.082	–0.064	–0.043	–0.031	–0.005	–0.177	0.000	0.010
	0.960	–0.419	–0.351	–0.298	–0.280	–0.228	0.020	0.060	0.030	0.090	0.110
0.48	0.000	1.110	1.195	1.220	1.192	1.091	1.430	1.443	1.430	1.378	1.374
	0.025	–0.594	–0.322	–0.091	0.110	0.330	0.170	0.270	0.430	0.450	0.530
	0.050	–0.690	–0.554	–0.341	–0.154	0.040	–0.049	0.040	0.210	0.210	0.290
	0.075	–0.808	–0.664	–0.468	–0.293	–0.110	–0.172	–0.083	0.070	0.070	0.140
	0.100	–0.892	–0.756	–0.570	–0.419	–0.227	–0.273	–0.180	–0.027	–0.047	0.010
	0.125	–0.950	–0.823	–0.654	–0.502	–0.315	–0.364	–0.265	–0.121	–0.152	–0.092
	0.150	–0.889	–0.780	–0.645	–0.497	–0.282	–0.413	–0.308	–0.176	–0.213	–0.160
	0.210	–0.426	–0.206	–0.106	–0.129	–0.100	–0.256	–0.212	–0.216	–0.134	–0.073
	0.260	–0.198	–0.155	–0.179	–0.181	–0.133	–0.127	–0.083	–0.028	–0.026	0.020
	0.320	–0.311	–0.313	–0.296	–0.248	–0.186	–0.082	–0.063	–0.024	–0.064	–0.027
	0.370	–0.241	–0.305	–0.304	–0.198	–0.106	–0.102	–0.090	–0.012	–0.094	–0.058
	0.420	–0.145	–0.145	–0.133	–0.118	–0.087	–0.095	–0.076	–0.009	–0.088	–0.052
	0.470	–0.153	–0.143	–0.130	–0.113	–0.091	–0.145	–0.140	–0.049	–0.150	–0.110
	0.540	–0.138	–0.137	–0.119	–0.107	–0.085	–0.181	–0.168	–0.084	–0.168	–0.127
	0.600	–0.107	–0.104	–0.099	–0.086	–0.056	–0.219	–0.192	–0.113	–0.199	–0.174
	0.700	–0.096	–0.089	–0.085	–0.070	–0.043	–0.269	–0.242	–0.170	–0.226	–0.197
	0.800	–0.088	–0.087	–0.075	–0.061	–0.033	–0.315	–0.289	–0.193	–0.168	–0.115
	0.900	–0.104	–0.115	–0.102	–0.075	–0.033	0.000	0.000	–0.124	–0.008	0.000
	0.960	–0.163	–0.160	–0.184	–0.185	–0.189	0.070	0.070	–0.113	0.100	0.140
0.86	0.000	1.104	1.183	1.188	1.138	1.025	1.429	1.450	1.418	1.332	1.326
	0.025	–0.517	–0.357	–0.159	0.020	0.240	0.130	0.230	0.370	0.370	0.460
	0.050	–0.768	–0.593	–0.398	–0.232	–0.054	–0.077	–0.002	0.150	0.130	0.200
	0.075	–0.714	–0.603	–0.456	–0.343	–0.206	–0.184	–0.120	0.030	0.000	0.060
	0.100	–0.696	–0.633	–0.535	–0.450	–0.322	–0.258	–0.205	–0.063	–0.104	–0.051
	0.125	–0.717	–0.654	–0.579	–0.498	–0.378	–0.298	–0.244	–0.129	–0.177	–0.131
	0.150	–0.740	–0.687	–0.585	–0.459	–0.329	–0.329	–0.280	–0.189	–0.238	–0.194
	0.210	–0.321	–0.097	–0.085	–0.126	–0.140	–0.270	–0.192	–0.167	–0.209	–0.173
	0.260	–0.125	–0.124	–0.145	–0.146	–0.143	–0.258	–0.179	–0.111	–0.146	–0.072
	0.320	–0.196	–0.181	–0.176	–0.153	–0.117	0.000	0.000	–0.119	0.000	0.030
	0.370	–0.222	–0.205	–0.184	–0.147	–0.115	–0.008	–0.001	0.040	–0.042	–0.018
	0.420	–0.160	–0.152	–0.125	–0.108	–0.094	–0.038	–0.030	0.030	–0.082	–0.068
	0.470	–0.147	–0.131	–0.106	–0.100	–0.090	–0.061	–0.064	–0.018	–0.105	–0.084
	0.540	–0.156	–0.129	–0.098	–0.091	–0.089	–0.106	–0.088	–0.056	–0.117	–0.114
	0.600	–0.153	–0.112	–0.089	–0.071	–0.071	–0.126	–0.119	–0.077	–0.128	–0.099
	0.700	–0.169	–0.107	–0.076	–0.065	–0.061	–0.170	–0.149	–0.091	–0.149	–0.136
	0.800	–0.177	–0.102	–0.068	–0.063	–0.059	–0.219	–0.191	–0.116	–0.153	–0.136
	0.900	–0.122	–0.027	–0.004	–0.018	–0.027	–0.054	0.010	–0.068	0.060	0.080
	0.960	–0.274	–0.208	–0.172	–0.166	–0.177	–0.109	–0.100	–0.206	–0.100	–0.051

Table C-6. Chordwise pressure distribution data, obtained in flight, as a function of angle of attack.

		M ≈ 0.54, Hp ≈ 30,000 ft			
	α	−1.85	0.30	2.19	4.05
	β	−0.21	−0.42	−0.27	−0.26
z/b	*x/c*				
0.16	0.000	1.029	1.034	1.023	1.000
	0.025	−0.127	−0.104	−0.104	−0.103
	0.050	−0.210	−0.197	−0.189	−0.182
	0.075	−0.221	−0.196	−0.197	−0.192
	0.100	−0.238	−0.223	−0.214	−0.202
	0.125	−0.215	−0.203	−0.189	−0.186
	0.150	−0.167	−0.159	−0.145	−0.148
	0.210	−0.103	−0.087	−0.081	−0.069
	0.260	−0.134	−0.119	−0.112	−0.099
	0.320	−0.102	−0.086	−0.084	−0.080
	0.370	−0.075	−0.067	−0.058	−0.054
	0.420	−0.059	−0.053	−0.048	−0.050
	0.470	−0.068	−0.054	−0.050	−0.055
	0.540	−0.062	−0.055	−0.047	−0.051
	0.600	−0.033	−0.025	−0.027	−0.028
	0.700	−0.011	−0.011	−0.011	−0.020
	0.800	−0.024	−0.020	−0.030	−0.047
	0.900	−0.028	−0.030	−0.043	−0.063
	0.960	−0.136	−0.148	−0.166	−0.189
0.48	0.000	1.033	1.039	1.029	1.007
	0.025	−0.141	−0.124	−0.120	−0.124
	0.050	−0.252	−0.231	−0.232	−0.223
	0.075	−0.271	−0.248	−0.248	−0.247
	0.100	−0.276	−0.256	−0.250	−0.241
	0.125	−0.276	−0.258	−0.257	−0.252
	0.150	−0.208	−0.201	−0.189	−0.189
	0.210	−0.095	−0.087	−0.074	−0.082
	0.260	−0.071	−0.060	−0.054	−0.053
	0.320	−0.095	−0.080	−0.079	−0.083
	0.370	−0.047	−0.039	−0.037	−0.042
	0.420	−0.034	−0.023	−0.025	−0.026
	0.470	−0.034	−0.027	−0.027	−0.033
	0.540	−0.026	−0.022	−0.026	−0.022
	0.600	−0.016	−0.014	−0.018	−0.031
	0.700	−0.015	−0.013	−0.015	−0.026
	0.800	−0.017	−0.019	−0.024	−0.036
	0.900	−0.046	−0.047	−0.059	−0.073
	0.960	−0.093	−0.090	−0.110	−0.135
0.86	0.000	0.990	0.990	0.980	0.920
	0.025	−0.151	−0.125	−0.106	−0.098
	0.050	−0.240	−0.213	−0.207	−0.197
	0.075	−0.255	−0.229	−0.217	−0.197
	0.100	−0.250	−0.230	−0.211	−0.213
	0.125	−0.222	−0.208	−0.197	−0.187
	0.150	−0.182	−0.169	−0.166	−0.163
	0.210	−0.071	−0.057	−0.061	−0.060
	0.260	−0.053	−0.046	−0.041	−0.044
	0.320	−0.025	−0.020	−0.023	−0.026
	0.370	−0.047	−0.041	−0.042	−0.051
	0.420	−0.026	−0.015	−0.026	−0.028
	0.470	−0.025	−0.019	−0.022	−0.034
	0.540	−0.020	−0.013	−0.026	−0.045
	0.600	−0.016	−0.011	−0.023	−0.034
	0.700	−0.010	−0.005	−0.014	−0.037
	0.800	−0.017	−0.010	−0.030	−0.049
	0.900	−0.022	−0.022	−0.033	−0.046
	0.960	−0.120	−0.125	−0.142	−0.176

APPENDIX D
BOUNDARY-LAYER PROFILE DATA

Table D-1. Steady-state boundary-layer profile data obtained in flight, $Hp \approx 15{,}000$ ft.

	Free-stream Mach number						
y (in.)	0.39	0.52	0.61	0.70	0.80	0.90	0.98
0.025	0.583	0.592	0.599	0.613	0.596	0.606	0.590
0.040	0.633	0.652	0.655	0.653	0.658	0.638	0.635
0.095	0.691	0.694	0.705	0.714	0.709	0.701	0.689
0.150	0.709	0.714	0.728	0.740	0.743	0.738	0.713
0.190	0.744	0.747	0.756	0.764	0.773	0.762	0.746
0.250	0.768	0.762	0.780	0.787	0.790	0.793	0.768
0.290	0.794	0.788	0.794	0.797	0.809	0.806	0.775
0.350	0.800	0.791	0.807	0.817	0.823	0.823	0.804
0.400	0.826	0.823	0.821	0.829	0.839	0.833	0.813
0.500	0.847	0.848	0.851	0.855	0.860	0.862	0.844
0.650	0.909	0.919	0.909	0.907	0.911	0.916	0.900
0.850	0.945	0.954	0.956	0.954	0.955	0.956	0.941
1.000	0.968	0.979	0.981	0.981	0.981	0.985	0.981
1.250	0.984	0.988	0.992	0.995	0.996	0.996	0.996
1.450	0.994	0.998	0.996	0.998	0.999	0.997	1.000
1.650	0.991	0.994	0.995	0.998	0.999	0.997	0.999
1.900	0.992	0.996	0.996	0.998	0.999	0.998	0.998
2.100	0.994	0.997	0.997	0.999	1.000	0.998	0.998
2.300	0.989	0.996	0.997	0.998	0.998	0.999	0.998
2.500	0.983	0.994	0.995	0.998	0.999	1.000	0.997
M_τ	0.42	0.53	0.64	0.76	0.85	0.95	0.99
T_f	497.7	506.6	517.1	530.6	543.5	559.7	569.5
T_w	527.1	535.0	543.6	548.8	552.6	555.2	556.3
P_w	1194.3	1180.7	1168.2	1157.5	1153.5	1166.7	1205.5

Table D-2. Steady-state boundary-layer profile data obtained in flight, $Hp \approx 30{,}000$ ft.

	Free-stream Mach number										
y (in.)	0.51	0.62	0.70	0.79	0.89	1.00	1.05	1.15	1.28	1.39	1.48
0.025	0.566	0.582	0.580	0.583	0.576	0.562	0.535	0.551	0.156	0.070	0.188
0.040	0.625	0.618	0.645	0.635	0.635	0.617	0.593	0.588	0.285	0.276	0.306
0.095	0.682	0.677	0.696	0.691	0.687	0.664	0.649	0.631	0.375	0.409	0.450
0.150	0.711	0.706	0.726	0.730	0.712	0.694	0.676	0.654	0.441	0.500	0.504
0.190	0.742	0.739	0.751	0.754	0.746	0.722	0.705	0.684	0.523	0.599	0.599
0.250	0.758	0.762	0.772	0.773	0.771	0.750	0.726	0.706	0.568	0.656	0.663
0.290	0.767	0.774	0.790	0.789	0.792	0.757	0.738	0.718	0.603	0.695	0.703
0.350	0.787	0.796	0.811	0.807	0.810	0.778	0.766	0.745	0.659	0.738	0.757
0.400	0.808	0.813	0.823	0.816	0.820	0.787	0.777	0.759	0.683	0.764	0.780
0.500	0.835	0.841	0.852	0.848	0.849	0.818	0.822	0.796	0.761	0.813	0.841
0.650	0.893	0.900	0.908	0.901	0.902	0.885	0.876	0.859	0.851	0.886	0.901
0.850	0.942	0.948	0.950	0.949	0.950	0.929	0.940	0.915	0.914	0.926	0.934
1.000	0.961	0.977	0.980	0.977	0.971	0.970	0.973	0.957	0.955	0.955	0.963
1.250	0.979	0.990	0.993	0.994	0.991	0.993	0.995	0.988	0.989	0.981	0.987
1.450	0.993	0.994	0.999	0.999	0.997	0.999	0.999	0.999	1.000	1.000	0.992
1.650	0.989	0.993	0.997	0.997	0.997	0.999	1.000	1.000	0.998	0.989	0.994
1.900	0.994	0.996	0.998	0.998	0.998	0.999	0.999	0.999	0.995	0.986	0.997
2.100	1.000	1.000	1.000	1.000	0.998	1.000	0.999	0.999	0.991	0.982	1.000
2.300	0.989	0.994	0.997	0.997	1.000	0.998	0.998	0.997	0.979	0.981	0.999
2.500	0.979	0.994	0.997	0.999	0.999	0.998	0.997	0.997	0.977	0.982	0.998
M_τ	0.53	0.65	0.75	0.84	0.93	1.00	1.01	1.09	1.27	1.55	1.71
T_f	435.2	445.1	455.4	465.6	477.5	490.6	503.8	526.6	548.7	558.9	593.1
T_w	486.2	494.7	500.3	504.6	508.9	515.1	521.5	526.7	528.4	526.5	523.1
P_w	647.6	638.8	634.4	629.2	635.0	663.7	711.3	743.1	645.0	606.1	603.4

Table D-3. Steady-state boundary-layer profile data obtained in flight, $Hp \approx 45{,}000$ ft.

	Free-stream Mach number													
y (in.)	0.70	0.79	0.90	0.98	1.06	1.16	1.28	1.39	1.49	1.60	1.69	1.80	1.90	2.00
0.025	0.568	0.573	0.584	0.551	0.519	0.512	0.180	0.177	0.207	0.444	0.507	0.533	0.514	0.491
0.040	0.621	0.621	0.630	0.601	0.583	0.559	0.146	0.317	0.335	0.506	0.564	0.585	0.581	0.568
0.095	0.669	0.677	0.681	0.652	0.643	0.575	0.312	0.443	0.476	0.570	0.628	0.653	0.667	0.660
0.150	0.705	0.702	0.708	0.673	0.676	0.602	0.387	0.516	0.539	0.613	0.669	0.706	0.727	0.724
0.190	0.738	0.739	0.745	0.714	0.717	0.627	0.477	0.596	0.621	0.669	0.728	0.762	0.801	0.793
0.250	0.758	0.764	0.765	0.736	0.742	0.653	0.539	0.653	0.686	0.712	0.776	0.809	0.857	0.847
0.290	0.771	0.778	0.782	0.751	0.765	0.669	0.599	0.698	0.728	0.735	0.804	0.825	0.882	0.875
0.350	0.793	0.800	0.800	0.780	0.784	0.690	0.646	0.731	0.774	0.766	0.832	0.854	0.914	0.907
0.400	0.807	0.816	0.815	0.794	0.804	0.707	0.679	0.760	0.804	0.785	0.848	0.867	0.924	0.926
0.500	0.836	0.849	0.840	0.823	0.842	0.746	0.756	0.808	0.856	0.823	0.886	0.895	0.957	0.961
0.650	0.898	0.906	0.890	0.879	0.905	0.832	0.854	0.877	0.913	0.870	0.935	0.931	0.984	0.995
0.850	0.941	0.948	0.929	0.930	0.955	0.905	0.920	0.919	0.945	0.904	0.952	0.955	0.985	0.998
1.000	0.966	0.973	0.957	0.967	0.984	0.955	0.963	0.948	0.972	0.917	0.952	0.962	0.978	0.990
1.250	0.982	0.989	0.981	0.988	0.995	0.986	0.992	0.979	0.996	0.917	0.970	0.974	0.972	0.984
1.450	0.992	0.996	0.997	0.995	0.999	1.000	1.000	1.000	1.000	0.919	0.987	0.987	0.977	0.985
1.650	0.990	0.997	0.997	0.995	0.998	0.998	0.999	0.993	0.994	0.927	1.000	0.990	0.986	0.994
1.900	0.991	0.998	0.998	0.997	0.998	0.998	0.989	0.992	0.996	0.951	0.997	0.995	0.993	0.996
2.100	0.992	0.998	0.999	0.998	0.998	0.998	0.979	0.990	0.998	0.975	0.995	0.999	1.000	0.999
2.300	0.990	0.999	0.999	0.997	0.997	0.996	0.975	0.990	0.998	0.993	0.993	1.000	0.998	0.997
2.500	0.989	0.997	0.999	0.995	0.997	0.996	0.975	0.989	0.997	1.000	0.999	0.996	0.995	0.996
M_t	0.78	0.87	0.96	1.00	1.04	1.12	1.29	1.56	1.70	—	1.91	2.00	2.09	2.17
T_f	427.2	438.2	451.2	461.7	475.4	496.4	510.5	530.9	553.3	602.7	620.5	635.3	652.9	679.9
T_w	446.7	445.5	445.8	446.6	449.3	454.6	459.7	467.6	476.1	586.7	587.5	587.3	585.8	582.5
p_w	317.1	314.7	319.9	339.3	363.5	365.4	314.4	290.9	293.2	238.7	282.1	307.4	312.5	330.9

Table D-4. Boundary-layer profile data, obtained in flight, as a function of sideslip, Mach = 0.52 and 0.70.

	M = 0.52, $Hp \approx 15{,}000$ ft					M = 0.70, $Hp \approx 45{,}000$ ft				
β	8.04	3.95	0.00	-3.98	-8.00	8.02	4.01	-0.06	-3.98	-7.99
y (in.)										
0.025	0.686	0.626	0.577	0.629	0.688	0.712	0.631	0.555	0.629	0.654
0.040	0.729	0.681	0.628	0.675	0.707	0.761	0.683	0.614	0.650	0.688
0.095	0.775	0.775	0.684	0.705	0.739	0.817	0.751	0.670	0.704	0.737
0.150	0.834	0.804	0.709	0.731	0.783	0.839	0.765	0.693	0.730	0.752
0.190	0.863	0.840	0.732	0.778	0.795	0.884	0.810	0.746	0.759	0.781
0.250	0.893	0.860	0.772	0.796	0.822	0.908	0.821	0.754	0.785	0.812
0.290	0.910	0.884	0.796	0.810	0.852	0.935	0.844	0.773	0.796	0.832
0.350	0.924	0.893	0.819	0.832	0.872	0.955	0.875	0.795	0.819	0.839
0.400	0.947	0.897	0.831	0.842	0.880	0.973	0.877	0.814	0.837	0.864
0.500	0.975	0.928	0.863	0.863	0.905	0.985	0.907	0.843	0.875	0.899
0.650	0.998	0.981	0.902	0.921	0.957	0.999	0.952	0.909	0.921	0.950
0.850	0.989	0.985	0.951	0.964	0.987	1.000	0.955	0.947	0.963	0.973
1.000	0.996	0.965	0.974	0.986	0.997	0.993	0.944	0.972	0.982	0.991
1.250	0.989	0.971	0.988	0.995	0.996	0.996	0.945	0.992	0.988	0.987
1.450	1.000	0.963	0.996	0.995	0.997	0.999	0.970	0.993	0.989	0.999
1.650	0.996	0.969	0.997	0.995	0.997	0.985	0.981	0.991	0.988	0.990
1.900	0.980	0.976	0.997	0.996	0.997	0.966	0.986	0.989	0.989	0.991
2.100	0.965	0.983	0.998	0.997	0.996	0.947	0.990	0.986	0.991	0.991
2.300	0.952	0.996	0.998	0.998	0.997	0.935	0.960	0.973	0.990	0.997
2.500	0.928	1.000	1.000	0.996	0.994	0.922	0.936	0.960	0.991	0.994

Table D-5. Boundary-layer profile data, obtained in flight, as a function of angle of sideslip, Mach = 0.89 and 1.28.

	M = 0.89, $Hp \approx$ 45,000 ft					M = 1.28, $Hp \approx$ 45,000 ft				
β	7.96	3.99	–0.03	–3.82	–7.97	3.57	1.93	–0.07	–2.02	–3.59
y (in.)										
0.025	0.693	0.637	0.561	0.620	0.644	—	—	0.331	0.276	0.514
0.040	0.740	0.704	0.617	0.650	0.669	—	—	0.414	0.339	0.553
0.095	0.798	0.767	0.659	0.689	0.715	0.157	0.159	0.497	0.413	0.598
0.150	0.834	0.799	0.685	0.718	0.739	0.270	0.147	0.552	0.456	0.639
0.190	0.880	0.848	0.734	0.750	0.773	0.411	0.316	0.631	0.526	0.681
0.250	0.916	0.878	0.763	0.779	0.800	0.504	0.417	0.679	0.581	0.720
0.290	0.938	0.899	0.779	0.792	0.819	0.582	0.481	0.706	0.627	0.742
0.350	0.961	0.913	0.795	0.809	0.838	0.653	0.550	0.739	0.675	0.775
0.400	0.973	0.928	0.811	0.826	0.853	0.692	0.604	0.763	0.720	0.799
0.500	0.986	0.957	0.834	0.858	0.889	0.788	0.703	0.803	0.793	0.835
0.650	0.999	0.988	0.882	0.905	0.935	0.909	0.825	0.865	0.877	0.911
0.850	1.000	0.989	0.925	0.947	0.977	0.976	0.901	0.907	0.935	0.962
1.000	0.998	0.983	0.952	0.975	0.990	0.993	0.954	0.937	0.972	0.964
1.250	0.998	0.981	0.978	0.990	0.995	1.000	0.989	0.965	0.987	0.962
1.450	0.993	0.986	0.993	1.000	0.997	0.995	1.000	0.977	0.997	0.987
1.650	0.983	0.994	0.993	0.996	0.997	0.976	0.999	0.987	0.997	0.996
1.900	0.959	0.996	0.996	0.997	0.997	0.956	0.989	0.993	0.996	0.995
2.100	0.935	0.999	0.998	0.998	0.998	0.936	0.978	0.999	0.994	0.995
2.300	0.905	0.997	1.000	0.997	0.996	0.929	0.976	0.998	0.984	0.994
2.500	0.858	0.992	0.998	0.999	0.996	0.924	0.976	1.000	0.980	0.997

Table D-6. Boundary-layer profile data, obtained in flight, as a function of angle of attack, Mach ≈ 0.54, Hp ≈ 30,000 ft.

	M ≈ 0.54, $Hp \approx$ 30,000 ft			
α	–1.85	0.30	2.19	4.05
β	–0.21	–0.42	–0.27	–0.26
y (in.)				
0.025	0.588	0.583	0.572	0.599
0.040	0.636	0.631	0.631	0.681
0.095	0.687	0.682	0.708	0.736
0.150	0.722	0.702	0.746	0.778
0.190	0.746	0.752	0.773	0.805
0.250	0.773	0.764	0.793	0.833
0.290	0.780	0.793	0.833	0.837
0.350	0.803	0.809	0.846	0.865
0.400	0.818	0.817	0.855	0.882
0.500	0.849	0.836	0.881	0.912
0.650	0.904	0.903	0.954	0.952
0.850	0.951	0.958	0.989	0.953
1.000	0.980	0.974	0.995	0.944
1.250	0.994	0.991	1.000	0.940
1.450	1.000	0.995	0.999	0.940
1.650	0.994	1.000	0.984	0.946
1.900	0.997	1.000	0.982	0.964
2.100	0.999	1.000	0.980	0.982
2.300	0.992	0.996	0.962	0.994
2.500	0.999	0.991	0.960	1.000

REPORT DOCUMENTATION PAGE

Form Approved
OMB No. 0704-0188

1. AGENCY USE ONLY (Leave blank)	2. REPORT DATE	3. REPORT TYPE AND DATES COVERED
	December 1996	Technical Memorandum

4. TITLE AND SUBTITLE

F-15B/Flight Test Fixture II: A Test Bed for Flight Research

5. FUNDING NUMBERS

WU 505-68-52

6. AUTHOR(S)

David. M Richwine

7. PERFORMING ORGANIZATION NAME(S) AND ADDRESS(ES)

NASA Dryden Flight Research Center
P.O. Box 273
Edwards, California 93523-0273

8. PERFORMING ORGANIZATION REPORT NUMBER

H-2113

9. SPONSORING/MONITORING AGENCY NAME(S) AND ADDRESS(ES)

National Aeronautics and Space Administration
Washington, DC 20546-0001

10. SPONSORING/MONITORING AGENCY REPORT NUMBER

NASA TM-4782

11. SUPPLEMENTARY NOTES

12a. DISTRIBUTION/AVAILABILITY STATEMENT

Unclassified—Unlimited
Subject Category 02

12b. DISTRIBUTION CODE

13. ABSTRACT (Maximum 200 words)

NASA Dryden Flight Research Center has developed a second-generation flight test fixture for use as a generic test bed for aerodynamic and fluid mechanics research. The Flight Test Fixture II (FTF–II) is a low-aspect-ratio vertical fin-like shape that is mounted on the centerline of the F-15B lower fuselage. The fixture is designed for flight research at Mach numbers to a maximum of 2.0. The FTF–II is a composite structure with a modular configuration and removable components for functional flexibility. This report documents the flow environment of the fixture, such as surface pressure distributions and boundary-layer profiles, throughout a matrix of conditions within the F-15B/FTF–II flight envelope. Environmental conditions within the fixture are presented to assist in the design and testing of future avionics and instrumentation. The intent of this document is to serve as a user's guide and assist in the development of future flight experiments that use the FTF–II as a test bed. Additional information enclosed in the appendices has been included to assist with more detailed analyses, if required.

14. SUBJECT TERMS	15. NUMBER OF PAGES
Aerodynamic characterization, Boundary-layer pressures, F-15B aerodynamic test bed, F-15 directional stability, Flight test facility, Flight test fixture, Flow visualization, Surface pressure distributions	53
	16. PRICE CODE: A04

17. SECURITY CLASSIFICATION OF REPORT	18. SECURITY CLASSIFICATION OF THIS PAGE	19. SECURITY CLASSIFICATION OF ABSTRACT	20. LIMITATION OF ABSTRACT
Unclassified	Unclassified	Unclassified	Unlimited